ISSN : 0019-5693

INDIAN JOURNAL
OF
THEORETICAL PHYSICS

VOLUME 64 NOS. 1, 2

JANUARY, 2016 — JUNE, 2016

Published by the
CALCUTTA INSTITUTE OF THEORETICAL PHYSICS
(Formerly, Institute of Theoretical Physics)
"BIGNAN KUTIR"
4/1, MOHAN BAGAN LANE, KOLKATA-700 004

ISSN: 0019-5693

INDIAN JOURNAL
OF
THEORETICAL PHYSICS

VOLUME 64 **NOS. 1, 2**

JANUARY, 2016 – JUNE, 2016

Published by the

CALCUTTA INSTITUTE OF THEORETICAL PHYSICS

(Formerly, INSTITUTE OF THEORETICAL PHYSICS)

" BIGNAN KUTIR"

4/1, MOHAN BAGAN LANE, KOLKATA- 700 004

ISSN: 0019-5693

INDIAN JOURNAL
OF
THEORETICAL PHYSICS

[Founder President : Late Prof. K. C. Kar, D.Sc.]

VOLUME 64 **NOS. 1, 2**

JANUARY, 2016 – JUNE, 2016

Co-Published by the

WILCOX BOOKS & PERIODICALS CO.

8/2/A, NEOGIPARA ROAD, KOLKATA – 700 036

INDIAN JOURNAL
OF
THEORETICAL PHYSICS
" BIGNAN KUTIR"
4/1, MOHAN BAGAN LANE, KOLKATA- 700 004, INDIA

SUBSCRIPTION RATE

INDIA : (For Library & Institute)
₹ 1500.00 for Vol. 64, 2016 and onwards
FOREIGN : $ 350 for Vol. 64, 2016 and onwards
Drafts, Orders, Enquiries & Claim for Non-Receipt of Journal should be sent to :

WILCOX BOOKS & PERIODICALS CO.

8/2/A, NEOGIPARA ROAD
KOLKATA – 700 036 (INDIA)
Website : www.wilcoxjournals.com
E-mail : wilcoxbooks@yahoo.com
: wilcoxbooks@gmail.com
Phone : 91-3325771147
Mobile : 91-9231675520

C O N T E N T S

INDIAN JOURNAL OF THEORETICAL PHYSICS, VOL. 64, NOS. 1 & 2, 2016

A note on stimulus gravitational wave detection

Farrin Payandeh
Department of Physics, Payame Noor University (PNU),
P.O. BOX, 19395-3697 Tehran, Iran
E-mail : payandehfarrin92@gmail.com

(Received for publication in March, 2016)

[Abstract : In this paper, we show that by calculating appropriate cross-sectional coefficients for the waves, one can obtain applicable mathematical tools of projecting and integrating in the transverse areas. In this way, the mathematical configuration of what we have in mind for detecting the gravitational waves, will form. These mathematical tools, are used to construct a way of approach, to the gravitational waves detection methods].

Keywords: Gravitational wave, Stimulation, Detection, Observation

1. Introduction

One independent approach in modern physics of any symmetry considerations at all is the study of a gravitational wave. Just as one identifies as water waves small ripples rolling across the ocean, so one gives the name gravitational waves, to small ripples rolling across spacetime[1-5]. Spacetime is similar. Propagating through the universe, according to Einstein's theory, must be a complex pattern of small-scale ripples in the spacetime curvature. These ripples are produced by binary stars, by supernovae, by gravitational collapse, by explosions in galactic nuclei. Locally, one can ignore the interaction of these ripples with the large-scale curvature of spacetime and their nonlinear interaction with each other. One can pretend the waves propagate in flat spacetime; and one can write down a simple wave equation for them. But globally one cannot. The large-scale curvature due to quiescent stars and galaxies will produce redshifts and will deform wave fronts; and the energy carried by the waves themselves will help to produce the large-scale curvature. The gravitational waves of our universe as propagating through flat, empty spacetime (local viewpoint).

Then they can be analyzed using the linearized theory of gravity, which has an extant availability in texts on general relativity and its astrophysical consequences[6-10]. Linearized theory, one recalls, is a weak-field approximation to general relativity. The equations of linearized theory are written and solved as though spacetime were flat (special-relativity viewpoint); but the connection to experiment is made through the curved-space formalism of general relativity.

In the recent years, a huge attempt has been devoted to detect the gravitational waves, which finally led to their detection[11] in 2016. A gravitational wave detector is even easier to analyze than the generator (for example, a binary system or a black-hole) when one deals with gravitational waves within the framework of general relativity. Potential detectors are usually installed in the solar system, where gravity is so weak and spacetime so nearly flat that a plane gravitational wave coming in, remains for all practical purposes a plane gravitational wave. Moreover, the nearest source of significant waves is so far away that, for all practical purposes, one can consider the waves as plane-fronted when they reach the Earth. Consequently, as they propagate in the Z-direction past a detector, they can be described to high accuracy by the transverse-traceless linearized expressions. Because of the increasing importance of constructing gravitational waves detectors, In this paper as well, we deal with the possible ways of building such detectors, in a mathematical viewpoint. The paper is organized as follows: In Sec. 2, we consider a resonant detector based on a definite pattern of an ideal detector. In Sec. 3, we assume that this detector obeys polarized wave equations in the $E_{\text{vibration}} \gg kT$ limit. In Sec. 4, we take into account small displacements and solve the wave equations which results in the determinations of the massive approximation. We conclude in Sec. 5.

2. The Idealized Resonant Detector

We consider the proper reference frame of a vibrating-bar detector. In such detectors, the bar hangs by a wire from a cross beam, which is supported by vertical posts (see Fig. 1) that are embedded in the Earth. Consequently, the bar experiences a 4-acceleration given, by $\boldsymbol{a} = g(\partial / \partial \hat{z})$,

where g is the local acceleration of gravity. Later, the spatial axes will have rotated relative to the bar, so the components of $\boldsymbol{a}$ but not its magnitude will have changed. The proper reference frame relies on an imaginary clock and three imaginary gyroscopes located at the bar's center of mass. Coordinate time is equal to proper time as measured by the clock, and the directions of the spatial axes $\partial/\partial x^{\hat{j}}$ are attached to the gyroscopes. The forces that prevent the gyroscopes from falling in the Earth's field must be applied at the centers of mass of the individual gyroscopes.

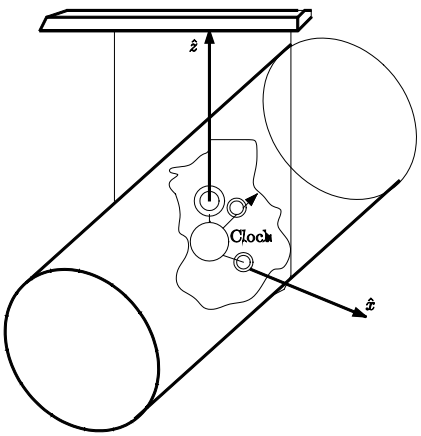

Fig.1
A schematic view of the vibrating bar detector.

The metric perturbation

$$h_{xx}^{TT} = -h_{yy}^{TT} = A_{+}(t-z), h_{xy}^{TT} = h_{yx}^{TT} = A_{\times}(t-z), \quad \ldots \quad (1)$$

results in the Riemann tensor perturbations

$$R_{x0x0} = -R_{y0y0} = -\frac{1}{2}\ddot{A}_{+}(t-x),$$

$$R_{x0y0} = R_{y0x0} = -\frac{1}{2}\ddot{A}_{\times}(t-z). \quad \ldots \quad (2)$$

These together, give the following stress-energy tensor :

$$T_{00}^{(GW)} = T_{zz}^{(GW)} = -T_{0z}^{(GW)} = \frac{1}{16\pi}\left\langle \dot{A}_{+}^{2} + \dot{A}_{\times}^{2} \right\rangle_{\text{time average}} \quad \ldots \quad (3)$$

To analyze most easily the response of the detector to these impinging waves, use not the *TT* coordinate system $\{x^{\alpha}\}$ (which is specially "tuned" to the waves), but rather use coordinates $\{x^{\hat{\alpha}}\}$, specially "tuned" to the experimenter and his detector. The detector might be a vibrating bar, or the vibrating Earth, or a loop of tubing filled with fluid. But whatever it is, it will have a center of mass. Attached the spatial origin, $x^{\hat{j}}=0$, to this center of mass; and attach orthonormal spatial axes, $\partial/\partial x^{\hat{j}}$, to gyroscopes located at this spatial origin. If the detector is accelerating (*i.e.*, not falling freely on a geodesic curve), make the gyroscopes accelerate with it by applying the necessary forces at their centers of mass. Use, as time coordinate, the proper time $x^{\hat{0}}=\tau$ measured by a clock at the spatial origin. Finally, extend these locally defined coordinates $x^{\hat{\alpha}}$ throughout all spacetime in the straightest manner possible.

Now let the 4-velocity, *i.e.* the tangential vector to the trajectory curve, measured by an observer. Whose proper time is measured by the parameter τ, be denoted by u^{α}. The whole system would therefore obey the evolution equations[13-17].

$$\frac{d\Theta}{d\tau}+\frac{1}{3}\Theta^2+\sigma^2-\omega^2=-R_{\mu\nu}u^{\mu}u^{\nu},$$

$$\frac{d\sigma_{\mu\nu}}{d\tau}=-\frac{2}{3}\Theta\sigma_{\mu\nu}-\sigma_{\mu\lambda}\sigma^{\lambda}{}_{\nu}-\omega_{\mu\lambda}\omega^{\lambda}{}_{\nu}+\frac{1}{3}h_{\mu\nu}\left(\sigma^2-\omega^2\right)$$
$$+C_{\lambda\nu\mu\rho}u^{\lambda}u^{\rho}+\frac{1}{2}h_{\mu\lambda}h_{\nu\rho}R^{\lambda\rho}-\frac{1}{3}h_{\mu\nu}h_{\lambda\rho}R^{\lambda\rho},$$

$$\frac{d\omega_{\mu\nu}}{d\tau}=-\frac{2}{3}\Theta\omega_{\mu\nu}-2\sigma^{\lambda}{}_{[\nu}\omega_{\mu]\lambda}, \qquad \ldots \quad (4)$$

in which, $\Theta,\sigma_{\mu\nu}$ and $\omega_{\mu\nu}$ are respectively the scalar expansion, the symmetric traceless shear tensor and the anti-symmetric rotation tensor. Moreover $\sigma^2=\sigma_{\mu\nu}\sigma^{\mu\nu},\omega^2=\omega_{\mu\nu}\omega^{\mu\nu}$ and $C_{\lambda\nu\mu\rho}$ is the Weyl conformal tensor. Also $h_{\mu\nu}$ is the projection tensor which for time-like curves is defined by

$$h_{\mu\nu}=g_{\mu\nu}+u_{\mu}u_{\nu}. \qquad \ldots \quad (5)$$

Generally speaking, the equations (4) deal with the kinematics of flows which are generated by vector fields. Such flows are indeed congruences of integral curves which may or may not be geodesics. Actually in the context of these equations, we are interested in the evolution of the kinematical characteristics of the so-called flows, not the origin of them. These characteristics which are contained in those equations, may constitute one equation[18] like.

$$\nabla_\nu v_\mu = \sigma_{\mu\nu} + \omega_{\mu\nu} + \frac{1}{3} h_{\mu\nu}\Theta,$$

$$\sigma_{\mu\nu} = \nabla_{(\nu} v_{\mu)} - \frac{1}{3} h_{\mu\nu}\Theta,$$

$$\Theta = \nabla_\mu v^\mu, \qquad \ldots \quad (6)$$

and the antisymmetric part is

$$\omega_{\mu\nu} = \nabla_{[\nu} v_{\mu]}. \qquad \ldots \quad (7)$$

Geometrically, these quantities are related to a cross-sectional area which encloses a definite number of integral curves and is orthogonal to them. Moving along the flow lines, this area may isotropically changes its size or being sheared or twisted, however it still holds the same number of flow lines. There are some analogies with elastic deformations. Here we should note that the evolution equations may be essentially regarded as identities, which become equations when they are for example used in spacetimes defined by Einstein field equations. Moreover, thee equations are of first order and non-linear. Also the expansion equation, is the same as Riccati equation in mathematical regards[19]. The expansion is indeed the change of the cross-sectional area which is orthogonal to the geodesic (or non-geodesic) bundle.

Now for a detector which is falling on an integral curve in a weak gravitational system, the above formulations, do hold also when the waves impose small perturbations on the system. Regarding this, one can deal with the energy of the system, which the detector would feel. By using the advantage of the Hamilton-Jacobi equations, we have

$$g_{\mu\nu} p^\mu p^\nu + (mc)^2 = 0, \qquad \ldots \quad (8)$$

in which according to a parameterized trajectory bundle and in terms of the coordinates, p^{μ} is usually defined as[19]

$$p^{\mu} = \frac{dx^{\mu}}{d\tau} = \dot{x}^{\mu} \equiv u^{\mu}. \quad \ldots \quad (9)$$

For a typical spherical metric

$$ds^2 = g_{00}(dx^0)^2 + g_{rr}dr^2 + r^2 d\Omega^2, \quad \ldots \quad (10)$$

where $x^0 = ct$. For a conformal spherically symmetric metric, with $g_{00} = -B(r)$ and $g_{rr} = B(r)^{-1}$ where $B(r)$ is definitely dimensionless. One can write

$$\dot{x}^0 = \frac{a}{B(r)}. \quad \ldots \quad (11)$$

For pure radial geodesics curves, this gives

$$-B(r)\left(\dot{x}^0\right)^2 + B(r)^{-1}\left(\dot{r}\right)^2 + mc^2 = 0, \quad \ldots \quad (12)$$

Substitution of (11) and rearrangements result in

$$-\frac{1}{B(r)}\frac{a^2}{mc^2} + \frac{1}{B(r)}\frac{\dot{r}^2}{mc^2} + 1 = 0. \quad \ldots \quad (13)$$

Since each part of (15) has to be dimensionless, therefore we require that

$$\text{Dim}\,[a^2] = mc^2. \quad \ldots \quad (14)$$

Equation (13), hinging on the energy definition $E = -g_{00}p^0$, could be also written in the form

$$-\frac{1}{B(r)}\frac{E^2}{mc^2} + \frac{1}{B(r)}\frac{(p^r)^2}{mc^2} + 1 = 0. \quad \ldots \quad (15)$$

This shows an explicit dependence on energy of the curves for any kind of objects which move on such curves which also holds for a detector. In the next section, we will use these mathematical descriptions to describe a polarized gravitational wave equation and the consequent adjustments needed for the detectors to function appropriately.

3. The polarization limit and the adjustments

One can derive all the results for vibrating, resonant detectors. To pattern the derivation after the treatment of the idealized detector we should let it be wave-dominated ($E_{\text{vibration}} \gg KT$). We can show that the displacements $\delta x = \xi(x,t)$ of its mass elements are described by

$$\xi = \sum_n B_n(t) u_n(x), \qquad \ldots \quad (16)$$

where the time-dependent amplitude for the nth mode satisfies the driven-oscillator equation

$$\ddot{B}_n + \frac{\dot{B}_n}{\tau_n} + \omega_n^2 B_n = R_n(t), \qquad \ldots \quad (17)$$

and where the curvature-induced driving term is

$$R_n(t) = -\int (\frac{\rho}{M})\ u_n^j x^k d^3x = \frac{1}{4}\frac{\ddot{A}(\mp_{(n)jk} e_{jk})}{M} \qquad \ldots \quad (18)$$

To Fourier-analyze the amplitudes of the detector and waves, we have

$$\begin{aligned} B_n(t) &= (2\pi)^{-\frac{1}{2}} \int_{-\infty}^{+\infty} \tilde{B}_n(\omega) e^{-i\omega t} d\omega, \\ A(t) &= (2\pi)^{-\frac{1}{2}} \int_{-\infty}^{+\infty} \tilde{A}_n(\omega) e^{-i\omega t} d\omega, \end{aligned} \qquad \ldots \quad (19)$$

and solve the equation of motion (18) and (19), to obtain, in the neighborhood of resonance,

$$\tilde{B}_n = \frac{\frac{1}{8}\frac{\omega_n \tilde{A}(\mp_{(n)jk} e_{jk})}{M}}{|\omega| - \omega_n + \frac{1}{2}\frac{i}{\tau_n}} \qquad \text{for } |\omega \pm \omega_n| \ll \omega_n. \qquad \ldots \quad (20)$$

Also to calculate the total energy deposited in the detector by integrating

$$\begin{pmatrix} \text{energy} \\ \text{deposited} \end{pmatrix} = \int (\text{Force per unit volume}) \cdot (\text{Velocity})\, d^3x dt. \qquad \ldots \quad (21)$$

Thereby we obtain

$$\begin{pmatrix}\text{energy deposited in}\\ n-\text{th normal mode}\end{pmatrix}=\frac{1}{4}(I_{(n)\,jk}e_{jk})\int \ddot{A}\dot{B}_n\,dt. \qquad \ldots \quad (22)$$

We apply Parseval's theorem and combine with expression (19) to obtain[20-23].

$$\begin{pmatrix}\text{energy deposited in}\\ n-\text{th normal mode}\end{pmatrix}=\int \sigma_n(\nu)\mathcal{F}_\nu(\nu)d\nu, \qquad \ldots \quad (23)$$

where σ_n is given in Ref. [23], and (for $-\infty<\omega<+\infty$)

$$\mathcal{F}_\nu(\nu)=\mathcal{F}_\nu(\frac{\omega}{2\pi})=\frac{1}{8}\omega^2\,|\,\tilde{A}|^2\,. \qquad \ldots \quad (24)$$

It is shown that $\mathcal{F}_\nu(\nu)$ is the total energy per unit area per unit frequency carried by the waves past the detector[24-25]. One can obtain all the remaining cross sections by appropriate manipulations of this cross section[25]. In the next section. We use the mathematical tools for projecting out and integrating the transverse-traceless parts, which were developed the above discussions.

4. Solving the wave equations

The observed period of quadrupole vibration of the earth is 54 minutes[26-27]. To analyze that mode of vibration, with all due allowance for elasticity and the variation of density in the earth, is a major enterprise. Therefore, for a first estimate of the cross section of the earth for the absorption of quadrupole radiation, one can treat it as a globe of fluid of uniform density held in the shape of a sphere by gravitational forces alone (zero rigidity). Let the surface be displaced from $r=a$ to

$$r=a+a\;\alpha P_2(\cos\,\theta) \qquad \ldots \quad (25)$$

where θ is polar angle measured from the North Pole and α is the fractional elongation of the principal axis. The motion of lowestenergy compatible with this change of shape is described by the velocity field

$$\xi^x=-\frac{1}{2}\alpha x, \qquad \xi^y=-\frac{1}{2}\alpha y, \qquad \xi^x=\alpha z, \qquad \ldots \quad (26)$$

which implies zero divergence and zero curl. The sum of the kinetic energy and the gravitational potential energy is derived as

$$E = -\left(\frac{3}{5}\right)\left(\frac{M^2}{a}\right)\left(1-\frac{\alpha^2}{5}\right)+\left(\frac{3}{20}\right)Ma^2\ddot{\alpha}^2. \qquad \ldots \quad (27)$$

This shows that the angular frequency of the free quadrupole vibration is

$$\omega = \left(\frac{16\pi}{15}\right)^{\frac{1}{2}}\rho^{\frac{1}{2}}. \qquad \ldots \quad (28)$$

The reduced quadrupole moments are

$$I\!\!\!-_{xx} = I\!\!\!-_{yy} = \frac{Ma^2\alpha}{5}, \qquad I\!\!\!-_{zz} = \frac{2Ma^2\alpha}{5}. \qquad \ldots \quad (29)$$

Therefore the rate of emission of vibrational energy, averaged over a period, is

$$-\left\langle\frac{dE}{dt}\right\rangle = \left(\frac{3}{125}\right)M^2a^4\omega^6\alpha_{\text{peak}}^2. \qquad \ldots \quad (30)$$

In this regard, the exponential rate of decay of energy by reason of gravitational wave damping, or gravitational radiation line broadening, will be

$$A_{GW} = \left(\frac{4}{25}\right)Ma^2\omega^4. \qquad \ldots \quad (31)$$

Finally, the resonance integral of the absorption cross section for radiation incident from random directions with random polarization is

$$\int\langle\sigma(\nu)\rangle\,d\nu = \left(\frac{\pi}{2}\right)\lambda\!\!\!-^2A_{GW} = \left(\frac{2\pi}{25}\right)\frac{Ma^2}{\lambda\!\!\!-^2}. \qquad \ldots \quad (32)$$

By evaluating this resonance integral, this model of a globe of fluid of uniform density would imply for the earth, with average density $5.517\,\frac{gr}{cm^3}$, a quadrupole vibration period of 94 min, as compared to the observed 54 min; and a moment of inertia $(2/5)Ma^2$ as compared to the observed $0.33Ma^2$. These can be estimated as the correction factors for both effects and give for the final resonance integral $\sim 5\ cm^2Hz$.

5. Conclusion

In this paper, by considering a transverse-traceless configuration for a gravitational wave form, we calculated the perturbations for small displacements. This configurations was used in order to find applicable constructions for a gravitational wave detector, which is aimed to be installed in the solar system. The dynamic analysis of the idealized masses-on-spring detector, as developed in our investigations, is readily extended to a vibrating detector of arbitrary shape. The extension was carried out in Sec. 3 and its main results are summarized in Sec. 4. Part of the energy that goes into a detector is reradiated as scattered gravitational radiation. For any detector of laboratory dimensions with laboratory damping coefficients, this fraction is fantastically small. However, in principle one can envisage a larger system and conditions where the re-radiation is not at all negligible. In such an instance one is dealing with scattering. The attempt here, was made to analyze such scattering processes. For a simple order-of-magnitude treatment, one can use the same type of scattering formula that one employs to calculate the scattering of neutrons at a nuclear resonance or photons at an optical resonance. In conclusion, the detectors are heavily based on the stress-energy tensors of the system, which are imposed on the spacetime geometry and consequently, on the geometric congruences.

Acknowledgements

This work has been supported by Payame Noor University.

References

1. Greene, J., Bailyn, C.D. and Orosz J.A. – ApJ., **554**, 1290 (2001).
2. Fabian, A.C., Pringle, J.E. and Rees, M.J. – MNRAS, **172**, 15P (1975).
3. Fabian, A.C., Rees, M.J., Stella, L. and White, N.E. – MNRAS, **238**, 729 (1989).
4. Fabian, A.C. et al. – Nature, **459**, 540 (2009).
5. Jiang, J., Bambi, C. and Steiner, J.F. – JCAP, **5**, 025 (2015).
6. Jin, C., Ward, M., Done, C. and Gelbord, J.– MNRAS, **420**, 1825 (2012).
7. Esin, A.A., McClintock, J.E. and Narayan, R. – ApJ., **489**, 865 (1997).
8. Houck, J.C. and Denicola, L.A. – ASPC, **216**, 591 (2000).
9. Jin, C., Done, C., Middleton, M. and Ward, M. – MNRAS, **436**, 3173 (2013).
10. Brenneman, L.W. and Reynolds, C.S. – ApJ., **652**, 1028 (2006).

11. Abbott, B.P. et al. – Phys. Rev. Lett., **116**, 061102 (2016).
12. Fabian, A.C. – ARA&A, **50**, 455 (2012).
13. Greene, J.E. and Ho, L.C. – ApJ., **610**, 722 (2004).
14. Hubeny, I., Agol, E., Blaes, O. and Krolik, J.H. – ApJ., **533**, 710 (2000).
15. Jin, C., Ward, M. and Done, C. – MNRAS, **425**, 907 (2012).
16. Brenneman, L.W. et al. – ApJ., **736**, 103 (2011).
17. Hubeny, I., Blaes, O., Krolik, J.H. and Agol, E. – ApJ., **559**, 680 (2001).
18. Emmanoulopoulos, D., McHardy, I.M. and Papadakis, I.E. – MNRAS, **416**, L94 (2011).
19. Emmanoulopoulos, D., Papadakis, I.E., Dovciak, M. and McHardy, I.M. – MNRAS, **439**, 3931 (2014).
20. Jamil, O., Fender, R.P. and Kaiser, C.R. – MNRAS, **401**, 394 (2010).
21. Hubeny, I. and Lanz, T. – ApJ., **439**, 875 (1995).
22. Brenneman, L.W., Elvis, M., Krongold, Y., Liu, Y. and Mathur, S. –ApJ., **744**, 13 (2012).
23. Nayakshin, S., Power, C. and King, A.R. – ApJ., **753**, 15 (2012).
24. Narayan, R. and Yi, I. – ApJ., **428**, L13 (1994).
25. Narayan, R. and Yi, I. – ApJ., **444**, 231 (1995).
26. Nayakshin, S., Kazanas, D. and Kallman, T.R. – ApJ., **537**, 833 (2000).
27. Brito, R., Cardoso, V. and Pani, P. – Lecture Notes in Physics (Springer, Berlin, p. 906 (2015).

INDIAN JOURNAL OF THEORETICAL PHYSICS, VOL. 64, NOS. 1 & 2, 2016

Analysis of nonlinear Blasius equation to boundary layer flow over a flat plate

Ram Prakash Sharma[1,*], Madhu Jain[2] and Devendra Kumar[1]

[1]Department of Mathematics, JECRC University,
Jaipur-303905, Rajasthan, India
E-mail : ramprakash0808@gmail.com
: devendra.maths@gmail.com

[2]Department of Mathematics,
Indian Institute of Technology Roorkee, India
Email : madhufma@iitr.ac.in

(Received for publication in March, 2016)

[**Abstract :** The pivotal purpose of the present work is to study the issue related to an incompressible viscous flow over a flat plat. The homotopy analysis transform method is used to obtain the analytical approximate solution of the famous Blasius equation. The *HATM* is amalgamation of the homotopy analysis scheme, Laplace transform technique and homotopy polynomials. The suggested method is not limited to the small parameter such as in classical perturbation technique. The numerical results obtained with the help of proposed technique indicate that the method is very easy to use and computationally very strong.]

Keywords : Blasius equation; Flow over a flat plate; Homotopy analysis transform method; Viscous flow; Laplace transform method

1. Introduction

The Falkner-Skan equation is a nonlinear problem, whose solutions are the similarity solutions of 2-*D* incompressible laminar boundary layer equations. These type of two point boundary value problems cannot be solved directly in a closed form[1]. In a study Blasius[2] presented a solution in the form of power series. In an another work Howarth[3] employed the Runge-Kutta method to investigate the flat plate flow. Abussita[4] studied the

* Corresponding author : Tel. +91-9461070550

Blasius equation for a flow through a flat plate and established the existence of the solution. Further, Asaithambi[1] used the finite difference approach to obtain the numerical solution of the Falkner-Skan problem. In recent years Abbasbandy[5], Wang[6], Khoramishad and Mortezaei[7], Esmaeilpour and Ganji[8] and Ganjiet al.[9] studied the Blasius equation by using various analytical and numerical techniques.

The homotopy analysis method (*HAM*) was firstly propounded and developed by Liao[10-12]. It was successfully applied to 3-*D* boundary-layer nano fluid flow with heat transfer past a stretching sheet[13], *MHD* 3-*D* flow of viscoelastic nano fluid with nonlinear thermal radiation[14], magneto-hydrodynamic axisymmetric flow of third grade fluid through a stretching cylinder[15] and to some other fields, as well. Recently, many research workers combined the various analytical methods with the classical Laplace transform technique to develop new analytical techniques such as Laplace decomposition algorithm[16,17], homotopy perturbation transform scheme[18-20] and homotopy analysis transform method (*HATM*)[21-23].

The present study employs the *HATM* obtained analytical solution of Blasius equation. The *HATM* is an effective coupling of *HAM* and the well known Laplace transform algorithm, which is one of the most powerful and useful method for analytical solution with infinite boundary conditions. The *HATM* has an auxiliary parameter $\hbar$ for insuring the convergence of the solution. The results obtain by using the *HATM* are compared with the known results, which verifies the validity of the proposed approach.

2. Mathematical model of the problem

The boundary layer equations are taken in the form[24]:

$$\frac{\partial u}{\partial x}+\frac{\partial v}{\partial y}=0, \qquad \ldots \quad (1)$$

$$u\frac{\partial u}{\partial x}+v\frac{\partial u}{\partial y}=-\frac{1}{\rho}\frac{\partial p}{\partial x}+\nu\left(\frac{\partial^2 u}{\partial x^2}+\frac{\partial^2 u}{\partial y^2}\right), \qquad \ldots \quad (2)$$

$$u\frac{\partial v}{\partial x}+v\frac{\partial v}{\partial y}=-\frac{1}{\rho}\frac{\partial p}{\partial y}+\nu\left(\frac{\partial^2 v}{\partial x^2}+\frac{\partial^2 v}{\partial y^2}\right). \qquad \ldots \quad (3)$$

In the above equations *p* is independent of *z*. It is well known that a plate placed edgewise will not significantly disturb a uniform stream, as shown by practice in the presence of air and water, an ideal flow of primitive motive is the uniform flow[24]:

$$u \equiv U_\infty, \quad v \equiv 0 \qquad \text{for all } x, y. \qquad \ldots \quad (4)$$

The standard Blasius flat-plate problem is interpreted as that of obtaining a solution of Eqs. (1)-(3) varying from Eq. (4) only in the neighborhood of the plate the extent of which shrinks to zero as $v \to 0$. As the velocity of potential flow is assumed to be constant, consequently $\frac{dp}{dx} \equiv 0$. Therefore the boundary-layer equations takes the following form

$$\frac{\partial u}{\partial x} + \frac{\partial v}{\partial y} = 0, \qquad \ldots \quad (5)$$

$$u\frac{\partial u}{\partial x} + v\frac{\partial u}{\partial y} = \nu\frac{\partial^2 u}{\partial y^2} \qquad \ldots \quad (6)$$

$y = 0$: $u = v = 0$,

$y = \infty$: $u = U_\infty$. $\qquad \ldots \quad (7)$

Making use of a dimensionless variable (η) expressed as:

$$\eta = \frac{y}{\sqrt{x}} Re^{0.5}, \qquad \ldots \quad (8)$$

where *Re* indicates the Reynolds number and represented as:

$$Re = \frac{U_\infty x}{\nu}.$$

Thus the Eqs. (5)-(6) can be converted to popular Blasius equation

$$\frac{d^3 f}{d\eta^3} + \frac{1}{2} f \frac{d^2 f}{d\eta^2} = 0, \qquad \ldots \quad (9)$$

having the boundary conditions:

$$\eta = 0, \qquad f = \frac{df}{d\eta} = 0,$$

$$\eta \to \infty, \qquad \frac{df}{d\eta} = 1, \qquad \ldots \quad (10)$$

where f is related to u by $f = \frac{u}{U_\infty}$.

This is aparticular case of 2-*D* laminar boundary layer flows through a semi infinite flat plate which is given by Falkner-Skan equation:

$$\frac{d^3 f}{d\eta^3} + \frac{1}{2}(\mu+1) f \frac{d^2 f}{d\eta^2} + \mu\left[1 - \left(f(\eta)\right)^2\right] = 0, \qquad \ldots \quad (11)$$

with boundary conditions:

$$\eta = 0, \qquad f = \frac{df}{d\eta} = 0,$$

$$\eta \to \infty, \qquad \frac{df}{d\eta} = 1, \qquad \ldots \quad (12)$$

where μ is a constant.

For $\mu \geq 0$ there following cases arise:

$\mu = 0$: Blasius flow past a flat plate with a sharp edge.

$0 < \mu < 1$: Flow past a wedge with half angle $\theta_{1/2} = \mu\pi/(\mu+1)$ with $0 < \theta_{1/2} < \pi/2$.

$\mu = 1$: Heimenz flow in the direction of a plane stagnation point.

$1 < \mu < 2$: Flow into a corner with $\theta_{1/2} > \pi/2$.

$2 < \mu$: There is no simple ideal flow.

3. Basic idea of HATM

In order to demonstrated the solution process of the *HATM*, we take a 3rd order non-homogenous nonlinear ordinary differential equation having the initial conditions written as

$$f'''+b_1(x)f''+b_2(x)f'+b_3(x)f=g(f), \quad \ldots \quad (13)$$

$$f(0)=\alpha,\ \ f'(0)=\beta,\ \ f''(0)=\gamma, \quad \ldots \quad (14)$$

Applying the Laplace transform Eq. (13), we have

$$L[f''']+L[b_1(x)f''+b_2(x)f'+b_3(x)f]=L[g(f)]. \quad \ldots \quad (15)$$

On employing the differentiation property of the Laplace transform, it yields.

$$L[f]-\frac{\alpha}{s}-\frac{\beta}{s^2}-\frac{\gamma}{s^3}-\frac{1}{s^3}L[g(f)]+\frac{1}{s^3}L[b_1(x)f''+b_2(x)f'+b_3(x)f]=0. \quad \ldots \quad (16)$$

We express the nonlinear operator in the following form

$$N[\phi(\eta;q)]=L[\phi(\eta;q)]-\frac{\alpha}{s}-\frac{\beta}{s^2}-\frac{\gamma}{s^3}-\frac{1}{s^3}L[g(\phi(\eta;q))]$$

$$+\frac{1}{s^3}L[b_1(x)\varphi''(\eta;q)+b_2(x)\varphi'(\eta;q)+b_3(x)\varphi(\eta;q)]. \quad \ldots \quad (17)$$

In the Eq. (17) $q\in[0,1]$ and $\phi(\eta;q)$ is a function of η and q. The homotopy is developed as follows

$$(1-q)\,L[\phi(\eta;q)-f_0(\eta)]=\hbar\, qH(\eta)\,N[f(\eta)], \quad \ldots \quad (18)$$

where $H(\eta)\neq 0$ indicates an auxiliary function, $\hbar\neq 0$ represents an auxiliary parameter and $f_0(\eta)$ stands for an initial guess of $f(\eta)$. It is obvious that if the embedding parameter $q=0$ and $q=1$, it yields the following results

$$\phi(\eta;0)=f_0(\eta), \qquad \phi(\eta;1)=f(\eta), \quad \ldots \quad (19)$$

respectively. Thus, as q increases form 0 to1, the solution $\phi(\eta;q)$ varies from the initial guess $f_0(\eta)$ to the solution $f(\eta)$. Making use of Taylor series $\phi(\eta;q)$ is expressed as follow

$$\phi(\eta;q) = f_0(\eta) + \sum_{m=1}^{\infty} f_m(\eta)\, q^m, \qquad \ldots \quad (20)$$

where

$$f_m(\eta) = \frac{1}{m!}\frac{\partial^m \phi(\eta;q)}{\partial q^m}\Big|_{q=0}. \qquad \ldots \quad (21)$$

If the values of $f_0(\eta), \hbar$ and $H(\eta)$ are properly selected, the series (20) converges at q = 1, then we get

$$f(\eta) = f_0(\eta) + \sum_{m=1}^{\infty} f_m(\eta), \qquad \ldots \quad (22)$$

which must be one of the solutions of the given nonlinear equations. Using the definition[21], the governing equation can be derived from the zero-order deformation[18].

Define the vectors in the following manner

$$\vec{f}_m = \{f_0(\eta),\ f_1(\eta),\ldots,\ f_m(\eta)\}. \qquad \ldots \quad (23)$$

Differentiating the Eq. (18) m-times w.r. to q and after that dividing them by m! and lastly letting $q = 0,$ we have the subsequent deformation equation:

$$L[f_m(\eta) - \chi_m f_{m-1}(\eta)] = \hbar H(\eta)\Re_m(\vec{f}_{m-1}). \qquad \ldots \quad (24)$$

Using the inverse Laplace transform, we get

$$f_m(\eta) = \chi_m f_{m-1}(\eta) + \hbar L^{-1}[H(\eta)\Re_m(\vec{f}_{m-1})], \qquad \ldots \quad (25)$$

where

$$\Re_m(\vec{f}_{m-1}) = \frac{1}{(m-1)!}\frac{\partial^{m-1} N[\phi(\eta;q)]}{\partial q^{m-1}}\Big|_{q=0}, \qquad \ldots \quad (26)$$

and

$$\chi_m = \begin{cases} 0, & m \le 1, \\ 1, & m > 1. \end{cases} \quad \ldots \quad (27)$$

When $m \to \infty,$ we arrive at the accurate approximation of the Eq. (9)

$$f_m(\eta) = (\hbar + \chi_m) f_{m-1}(\eta) - \hbar(1-\chi_m)\left(\frac{\alpha}{s} + \frac{\beta}{s^2} + \frac{\gamma}{s^3}\right)$$

$$+ \hbar L^{-1}\left[\frac{1}{s^3} L\left(b_1(x)\right) f'' + b_2(x) f' + b_3(x) f - g(f)\right] \quad \ldots \quad (28)$$

In this manner, it is easily to be obtained $f_m(\eta)$ for $m \ge 1$ and approximate solution is given

$$f\ (\eta) = f_0(\eta) + k \to \infty \sum_{m=0}^{k} f_m(\eta), \quad \ldots \quad (29)$$

where

$$f_0(\eta) = f(0) + \eta \frac{df(0)}{d\eta} + \eta^2 \frac{d^2 f(0)}{d\eta^2} + \cdots$$

$$= \sum_{i=0}^{j} \eta^i \frac{\partial^{i-1} f(0)}{\partial \eta^{i-1}}. \quad \ldots \quad (30)$$

The nonlinear term *g(f)* is expanded in the form of homotopy polynomials as[25]

$$g(f) = \sum_{k=0}^{m} P_k\left(f_0, f_1, f_2, f_3, \cdots, f_k\right), \quad \ldots \quad (31)$$

where P_m are the homotopy polynomial which are calculated by the following formula

$$P_m\left(f_0, f_1, \cdots f_m\right) = \frac{1}{m!}\left[\frac{\partial^m g(q\phi_m(\eta;q))}{\partial \partial^m}\right]_{q=0}, m \ge 0. \quad \ldots \quad (32)$$

Combining Eqs. (28) and (31), we get

$$f_m(\eta) = (\hbar + \chi_m) f_{m-1}(\eta) - \hbar(1-\chi_m)\left(\alpha + \beta\eta + \frac{\gamma\eta^2}{2}\right) + \hbar L^{-1}\left[\frac{1}{s^3} L^{-1}\left(b_1(\eta) f''(\eta) + b_2(\eta) f'(\eta) + b_3(\eta) f(\eta) - \sum_{k=0}^{m-1} P_k\left(f_0, f_2, \cdots, f_k\right)\right)\right],$$

$$m = 1, 2, \ldots \qquad \ldots \quad (33)$$

From Eq. (33), we calculate $f_m(\eta)$ and substitute these values in (29), we obtain the analytical approximate solution of Eqs. (9)-(10). The novelty of our proposed algorithm is that a new functional (33) is constructed and is expanded the nonlinear form as a series of the homotopy polynomials.

4. Solution of the problem

To solve the Eqs. (9)-(10) by *HATM*, we apply the Laplace transform on Eq. (9), it yields

$$L[f] - \frac{a}{s^3} + \frac{1}{2}\frac{1}{s^3} L\left[f \frac{d^2 f}{d\eta^2}\right], \qquad \ldots \quad (34)$$

where $a = f''(0)$.

The nonlinear operator is

$$N[\phi(\eta;q)] = L[\phi(\eta;q)] - \frac{a}{s^3} + \frac{1}{2}\frac{1}{s^3} L\left[\phi(\eta;q)\frac{d^2}{d\eta^2}\phi(\eta;q)\right], \qquad \ldots \quad (35)$$

and thus

$$R_m(\vec{f}_{m-1}) = L[f_{m-1}] - (1-\chi_m)\frac{a}{s^3} + \frac{1}{2}\frac{1}{s^3} P_m\left(f_0, f_1, \cdots, f_{m-1}\right) \qquad \ldots \quad (36)$$

and the homotopy polynomials are given by

$$P_{m-1}\left(f_0, f_1, \cdots, f_{m-1}\right) = \sum_{r=0}^{m-1} f_{m-1-r} f_r''. \qquad \ldots \quad (37)$$

Using the initial approximation $f_0(\eta)=\frac{a\eta^2}{2}$ and the iterative scheme (25), we found the various components of the series solution:

$$f_1(\eta)=\frac{\hbar a^2}{2}\frac{\eta^5}{5!},$$

$$f_2(\eta)=\frac{\hbar}{2}(1+\hbar)\frac{a^2\eta^5}{5!}+\frac{1}{8!}\frac{11}{4}\hbar^2a^3\eta^8, \qquad \ldots \quad (38)$$

$$f_3(\eta)=\frac{\hbar}{2}(1+\hbar)^2\frac{a^2\eta^5}{5!}+\frac{1}{8!}\frac{41}{12}\hbar^2(1+\hbar)a^3\eta^8+\frac{375}{8}\frac{1}{11!}a^4\hbar^3\eta^{11},\cdots$$

Proceeding in the similar manner, the remaining of the iterates of the series solution can be completely derived and the solution is thus entirely obtained. Hence, the series solution when $\hbar=-1$ is

$$f(\eta)=-\frac{a^2}{2}\frac{\eta^5}{5!}+\frac{1}{8!}\frac{11}{4}a^3\eta^8-\frac{375}{8}\frac{1}{11!}a^4\eta^{11}+\cdots. \qquad \ldots \quad (39)$$

The value of a is evaluated by Howarth[3] using numerical technique. Inserting this value for $a=0.332057,$ into Eq. (39) yields the approximate solution of Blasius equation.

5. Convergence of the developed method

HATM series solution of Blasius equation (9) contains auxiliary parameter $\hbar$. This parameter has pivotal role in enhancing and managing the convergence of the solution of Blasius equation (9). To obtain a suitable range of $\hbar$ the $\hbar-$curve is shown in Fig. 1. From this Fig. 1, it is observed that suitable range for $\hbar$ is $-1.3\le\hbar\le-0.7.$

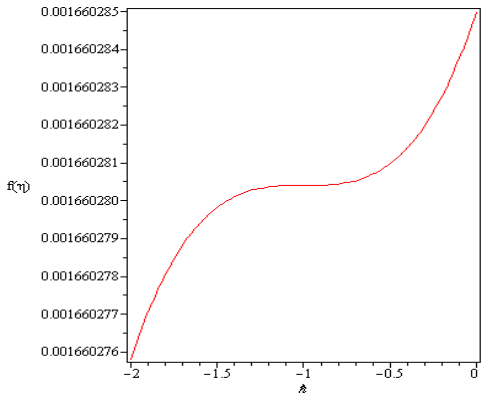

Figure 1
$\hbar-$curve for f at 3rd order of approximation.

6. *Results and discussions*

The numerical results were calculated up to three iterations and presented in Tables 1-2 and Figures 2-3. From the Tables 1-2, it can be seen that the results are in an excellent agreement with reported in data[8-9]. The Figures 2-3 depicts that the results obtained by the suggested approach are very near to the results obtained by Blasius[2].

Table 1
Comparative study between the results of *HATM*, *HPM*[9] and Numerical method[8] for $f(\eta)$.

η	*HATM*	*HPM*[9]	*NM*[8]
0.0	0	0	0
0.4	0.0265598	0.0265598	0.0266762
0.8	0.1061081	0.1061081	0.1061082
1.2	0.2379484	0.2379484	0.2379487
1.6	0.4203202	0.4203202	0.4203207
2.0	0.6500224	0.6500224	0.6500243
2.4	0.9222734	0.9222734	0.9222901
2.8	1.2308450	1.2308450	1.2309773
3.2	1.5682875	1.5682875	1.5690949
3.6	1.9255896	1.9255896	1.9295251
4.0	2.2897787	2.2897787	2.3057464

Table 2

Comparative study between the results of *HATM*, *HPM*[9] and Numerical method[8] for $f'(\eta)$.

η	*HATM*	*HPM*[9]	*NM*[8]
0.0	0	0	0
0.4	0.1327640	0.1327640	0.1327641
0.8	0.2647088	0.2647088	0.2647094
1.2	0.3937756	0.3937756	0.3937761
1.6	0.5167558	0.5167558	0.5167567
2.0	0.6297563	0.6297563	0.6297657
2.4	0.7288906	0.7288906	0.7289819
2.8	0.8108693	0.8108693	0.8115096
3.2	0.8726718	0.8726718	0.8760814
3.6	0.9087097	0.9087097	0.9233296
4.0	0.9027999	0.9027999	0.9555182

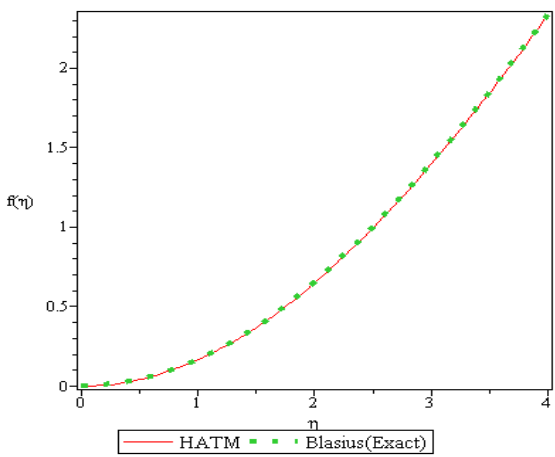

Figure 2

The comparison between the results obtained by *HATM* and Blasius[2] for $f(\eta)$.

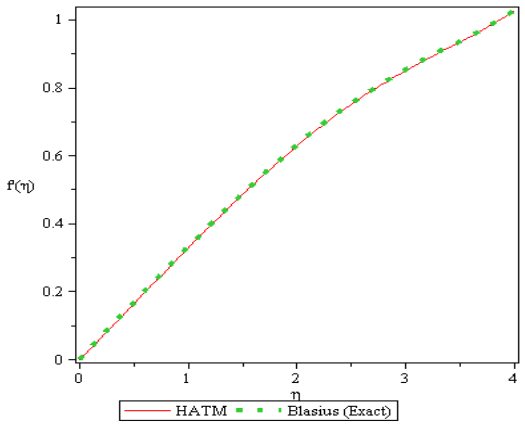

Figure 3

The comparison between the results obtained by *HATM* and Blasius[2] for $f'(\eta)$.

7. Concluding remarks

In this article we have analyzed the famous Blasius boundary layer equation. The *HATM* and symbolic computation have been used to solve the nonlinear differential equation. The results derived by the present method are in a very good agreement with the existing results. *HATM* gives us a very easy way to enhance and manage the region of convergence of the series solution by selecting proper value of $\hbar$. The results reveal that suggested scheme is a very efficient and computationally attractive approach to investigate nonlinear systems of physical significance.

References

1. Asaithambi, A. – A second order finite difference method for the Falkner-Skan equation, Applied Mathematics and Computation, **156,** 779-786 (2004).
2. Blasius, H.– Grenzschichten in Flussigkeiten mit kleiner reibung, Z. Math.u. Phys., **5 (1),** (1908).
3. Howarth, L.– On the solution of the laminar boundary layer equations, The Royal Soc. London, A **164 (919),** 547-579 (1938).
4. Abussita, A.M.M. – A note on a certain boundary layer equation, Applied Mathematics and Computation, **64(1),** 73-77 (1994).
5. Abbasbandy, S. – A numerical Solution of Blasius equation by Adomian's Decomposition Method and Comparison with Homotopy Perturbation Method, Chaos, Solitons and Fractals, **31,** 257-260 (2005).

6. Wang, L. –‘‘A New Algorithm for Solving Classical Blasius Equation”, Applied Mathematics and Computation,**157,** 1–9(2004).
7. Najafi, M., Khoramishad, H., Massah, H., Moghim, M. and Daemi, M.– A study of Blasius viscous flow: An ADM Analytical Solution, WSEAS Transactions on Mathematics, **5(7)**, 801-805 (2006).
8. Esmaeilpour, M. and Ganji, D.D. – Application of He’s homotopy perturbation method to boundary layer flow and convection heat transfer over a flat plate, Physics Letters, A **372 (1)**, 33-38 (2007).
9. Ganji, D. D.– An Application of Homotopy Perturbation Method for Non-linear Blasius Equation to Boundary Layer Flow Over a Flat Plate, International Journal of Nonlinear Science, **7(4)**, 399-404 (2009).
10. Liao, S. J. – Beyond Perturbation: Introduction to homotopy analysis method, Chapman and Hall / CRC Press, Boca Raton, (2003).
11. Liao, S.J. – On the homotopy analysis method for nonlinear problems, Applied Mathematics and Computation, **147**, 499–513 (2004).
12. Liao, S.J. – A new branch of solutions of boundary-layer flows over an impermeable stretched plate. International Journal of Heat and Mass Transfer, **48,** 2529-2539 (2005).
13. Zhao, Q. and Tao Fan,H.X.– Analysis of three-dimensional boundary-layer nanofluid flow and heat transfer over a stretching surface by means of the homotopy analysis method, Boundary Value Problems, **64**, DOI: 10.1186/s13661-015-0327-3(2015).
14. Hayat, T., Muhammad, T., Alsaedi, A. and Alhuthali, M.S. –Magnetohydrodynamic three-dimensional flow of viscoelastic nano fluid in the presence of nonlinear thermal radiation, Journal of Magnetism and Magnetic Materials, **385**, 222–229 (2015).
15. Hayat, T., Shaifq, A. and Alsaedi, A. – MHD axisymmetric flow of third grade fluid by a stretching cylinder, Alexandria Engineering Journal, **54 (2)**, 205–212 (2015).
16. Khuri, S.A. – A Laplace decomposition algorithm applied to a class of nonlinear differential equations, Journal of Applied Mathematics, **1,** 141–155 (2001).
17. Khan, M., Gondal, M.A. and Kumar, S.– A new analytical solution procedure for nonlinear integral equations, Mathematical and Computer Modelling, **55**, 1892–1897 (2012).
18. Gondal, M.A. and Khan, M.– Homotopy perturbation method for nonlinear exponential boundary layer equation using Laplace transformation, He’s polynomials and Pade technology, Int. J. Non. Sci. Numer. Simul., **11**, 1145−1153 (2010).
19. Singh, J., Kumar, D. and Kumar, S. – A reliable algorithm for solving discontinued problem arising in nanotechnology, Science Iranica, **20(3),** 1059–1062 (2013).

20. Singh, J., Kumar, D. and Kumar, S.– New treatment of fractional Fornberg-Whitham equation via Laplace transform, Ain Sham Engineering Journal, **4**, 557–562 (2013).

21. Khan, M., Gondal, M.A., Hussain, I. and Karimi Vanani, S. –A new comparative study between homotopy analysis transform method and homotopy perturbation transform method on semi-infinite domain, Mathematical and Computer Modelling, **55**, 1143–1150 (2012).

22. Kumar, D., Singh, J. and Sushila – Application of homotopy analysis transform method to fractional biological population model, Romanian Reports in Physics, **65(1)**, 63–75(2013).

23. Kumar, S., Kumar, D., Singh, J. and Kapoor, S. – New homotopy analysis transform algorithm to solve Volterra integral equation, A in Sham Engineering Journal, **5(1)**, 243-246 (2014).

24. Schlichting, H. – Boundary-layer Theory, The 7^{th} ed., McGraw-Hill Book Company, (1979).

25. Odibat, Z. and Bataineh, S.A.–An adaptation of homotopy analysis method for reliable treatment of strongly nonlinear problems: construction of homotopy polynomials, Math. Meth. Appl. Sci., DOI: 10.1002/mma.3136 (2014).

INDIAN JOURNAL OF THEORETICAL PHYSICS, VOL. 64, NOS. 1 & 2, 2016

Velocity profile and friction factor in a smooth pipe flow

B. C. Mandal*

Jalpaiguri Govt. Engineering College,
Jalpaiguri-735102,West Bengal, India
E-mail: bcmjgec@gmail.com

and

H. P. Majumdar

Retired Professor of Physics and Applied Mathematics Unit,
Indian Statistical Institute, Kolkata-700108, India

(Received for publication in April, 2016)

[**Abstract :** In this paper simple power law is used to describe structure of turbulent boundary layer in a pipe flow. Dependency of the power law constants on Reynolds Number is investigated. Friction factor is computed considering different velocity profiles. Computed friction factor is compared with the recent data.]

1. Introduction

The smooth pipe flow experimental data reported by McKeon have been dully exposed to the profession through published paper McKeon, et al.[1] Some velocity measurement data reported by McKeon et al.[1] (denoted *MK*) are plotted in Fig.1. The time mean velocity u is plotted along abscissa and corresponding distance y from the wall is plotted along ordinate. Only three measurements are plotted out of nineteen measurements in the Reynolds number, *Re* range, $7.4345E+04$ to $3.5724E+07$, where $Re = 2VR/\nu$, V = average velocity in the pipe, R = radius of the pipe and $\nu =$ kinematic viscosity of the fluid flowing through the pipe. No similarity is seen in the velocity profiles. It is seen that center line velocity U_c for the second profile (chronological order as given in the legend of Fig. 1) is higher than that of first profile. Consequently average velocity and Reynolds

*For Correspondence

number for the second profile is higher than that of first one as kinematic viscosity is nearly constant for two cases. Reynolds number for the third profile is highest though the centerline velocity is least. This is due to numerical value of the kinematic viscosity which is about 0.007 times the kinematic viscosity of the first and second profile. For the *MK* data, kinematic viscosity varies from $1.0854E-07$ to $1.5313E-05$.

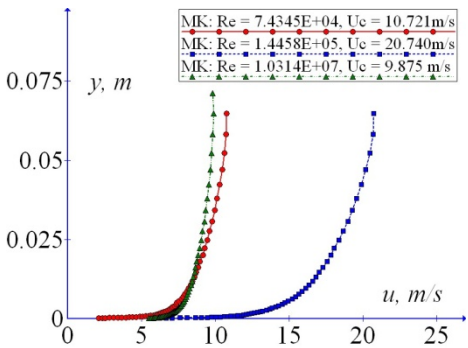

Fig. 1

Dimensional plot of velocity distribution in a smooth pipe.

Darcy deduced the following empirical velocity profile[2] on the basis of his careful measurements

$$\frac{U_c - u}{v_*} = 5.08\left(1-\frac{y}{R}\right)^{3/2} \qquad \ldots \quad (1)$$

where $U_c =$ velocity at the centerline of the pipe, time mean velocity u at a distance y from the wall, $v_* =$ shear velocity, and pipe radius R. It was pointed out in the literature that Darcy's formula gives good agreement at all points except those near the wall with $y/R < 0.25$. Eq. (1) is compared with the *MK* data and data of Hultmark et al.[3,4] (denoted *HK*) in Fig. 2. It is revealed that Eq. (1) gives good agreement with experimental data for $y/R > 0.5$ only.

Many formulas have been proposed latter to depict velocity distribution in a turbulent pipe flow. Pipe flow is also a kind of turbulent boundary layer problem. Hence, velocity distribution formulation for turbulent boundary

layer may be applicable to pipe flow also. Total velocity profile is generally divided into four regions: viscous sub-layer, buffer region, logarithmic region and outer region. However, broadly boundary layer may be divided into two regions only, *i.e.* wall/inner region and outer region. Inner region is consisting of viscous sub-layer, buffer region, and logarithmic region. Formula describes velocity distribution at the wall region is the "law of the wall" and "law of the wake" describes the flow at the outer region.

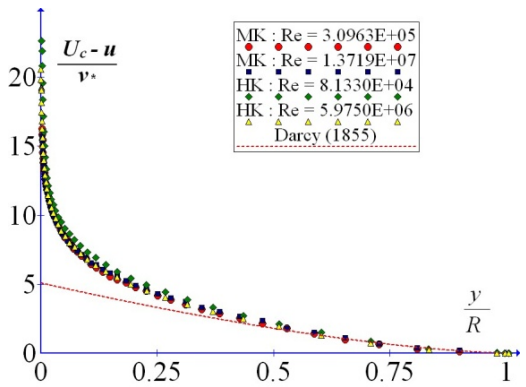

Fig. 2
Darcy's law compared with experimental data.

Law of the wall :

Prandtl[5] concluded that time mean velocity, u near the smooth wall must depend upon density ρ and viscosity μ of the fluid, the shear stress at the wall τ_w and on the distance from the wall, y. Thus, near the smooth wall there is a functional relationship

$$u = u(\rho, \mu, \tau_w, y) \qquad \ldots \quad (2)$$

From dimensional analysis the functional relationship can be written in the from

$$\frac{u}{v_*} = f\left(\frac{y v_*}{\nu}\right) \qquad \ldots \quad (3)$$

in which shear velocity, $v_* = \sqrt{\tau_w / \rho}$ and kinemetic viscosity, $\nu = \mu / \rho$. Introducing inner variables, $u^+ = u / v_*$ and $y^+ = y v_* / \nu$ equation (3) can be re-written as

$$u^+ = f(y^+) \qquad \ldots \quad (4)$$

Equation (4) is called law of the wall. Velocity data of *MK* and *HK* in a smooth pipe for *Re* range $7.4345E+04 \le Re \le 3.5724E+07$ and $8.1330E+04 \le Re \le 5.9750E+06$ respectively are plotted in terms of inner variables in Fig. 3.

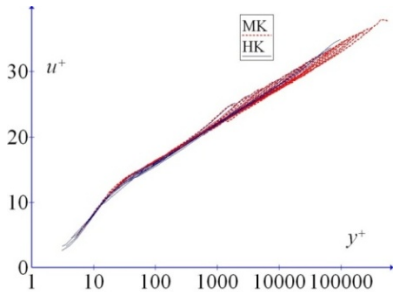

Fig. 3
Experimental profiles of mean velocity in terms of inner variables importance of plotting the profiles in terms of inner variables.

It is revealed that velocity profiles are self similar in the wall region and it supports the contention that the wall region is universal. On the other hand, profiles in the outer region depend on Reynolds number.

In Fig. 4, two velocity profiles from two different sources (*MK* and *HK*) having nearly equal Reynolds numbers but with different centerline velocities have been plotted. Figs. 3 and 4 show experimental evidence for the contention that the u^+, y^+ variables are indeed a good choice for describing the boundary layer and *Re* can be a reliable quantity to present the flow information.

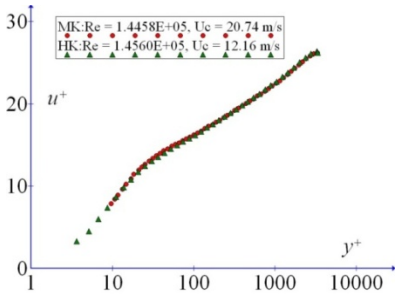

Fig. 4
Similarity of flows.

Very close to the wall, experimental data can be described by linear relationship, $u^+ = y^+$. This region is viscous sub-layer where viscous stress predominates. Prandtl[5] proposed logarithmic form of the law of the wall (Eq. (4)) for variation of velocity in the so-called overlap region at large distance from the wall

$$u^+ = \frac{1}{\kappa} \ln y^+ + B \qquad \ldots \quad (5)$$

which was derived analytically through his mixing length concept. The term κ is the von Karman constant and B is the constant of integration. The existence of the logarithmic law can be confirmed by Nikuradse[6] measurements on smooth pipe flow and constants $\kappa = 0.4$ and $B = 5.5$ can be obtained for the data[2]. In between the linear region and overlap region there is buffer region. Fig. 5 shows how the linear law and logarithmic law trace pipe flow data.

Area of controversy has been whether values of constants appearing in the logarithmic law are universal. Many values of κ and B can be found in the literature. Coles[7] considered value of $\kappa = 0.40$ and $B = 5.1$ in turbulent boundary layer computation, while Coles and Hirst[8] used $\kappa = 0.41$ and $B = 5$. Zagarola and Smits[9] analyzed their pipe flow data which led to the values of log-law constants $\kappa = 0.436$ and $B = 6.15$, whereas McKeon et al.[1] found $\kappa = 0.421$ and $B = 5.60$ (these values were used in Fig.5). Analyzing his zero pressure gradient turbulent boundary layer data, Osterlund et al.[10] found $\kappa = 0.38$ and $B = 4.1$. In case of channel flow, Zanoun et al.[11] fitted logarithmic law in overlap layer and found best fit for $\kappa = 0.379$ and $B = 4.05$.

The region described by the logarithmic law is called logarithmic region/overlap region where both, viscous and turbulent stresses are present. Region starting from the wall to the end the overlap region is called wall region. It is observed from Fig. 5, extent of the wall region depends on Reynolds number. Both laws, linear and logarithmic do not capture the data

points in the buffer region. Spalding[12] has given a special form of law of the wall

$$y^+ = f(u^+) = u^+ + A\left[e^{\kappa u^+} - 1 - \kappa u^+ - \frac{(\kappa u^+)^2}{2} - \frac{(\kappa u^+)^3}{6} - \frac{(\kappa u^+)^4}{24}\right] \quad \ldots \quad (6)$$

where $A = e^{-\kappa B}$ and value of κ and B can be used suitably. Fig.5 shows how Eq. (6) traces pipe flow data. It can be seen easily that the Spalding's formulation captures viscous sub-layer, buffer layer and logarithmic layer well without however describing the good trace of data points in the outer (wake) region. Spalding's formula has the undisputed advantage over the log-law that it is valid all the way to the wall where it satisfies the no-slip boundary condition. The unique feature of this law is that it represents y^+ as a function of u^+ rather than u^+ as a function of y^+. This feature has made computations using law of the wall much easier to perform.

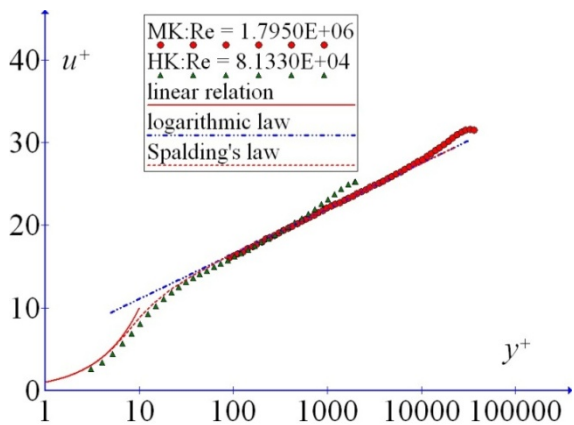

Fig. 5
Laws of the wall compared with experimental data.

Law of the wake :

Beyond the overlap region there is outer layer where influence of wall is absent in practical sense and turbulent stress predominates. Fig. 5 shows that experimental data at the outer region deviate from log law. This

deviation looks like a wake when viewed from the free stream. Existence of wake can be found in channel and pipe flow and in turbulent boundary layer but in varying amount. Logarithmic law and Spalding's law are too simple for describing the wake region. Accordingly, based on the idea of Coles[7], law of the wall should be replaced by

$$u^+ = f(y^+) + A(x)\, w(\eta) \qquad \ldots \quad (7)$$

where $A(x)$ is the amplitude function, $w(\eta)$ is the wake function and $\eta = y^+ / R^+ = y / R$, R being the radius of the pipe. The wake function is defined as the difference between the measured data in the outer region and extension of the logarithmic law in this region. Coles[7] proposed $A(x) = \Pi(x) / \kappa$, where $\Pi(x)$ is wake/profile parameter which is independent of the stream wise distance, x for uniform pipe and channel flow and the boundary layer on a flat plate subjected to zero pressure gradient. Hence, for pipe flow $\Pi(x)$ can be written as Π. Hinze[13] proposed empirical equation for wake function

$$w(\eta) = 2\sin^2\left(\frac{\pi}{2}\eta\right) \qquad \ldots \quad (8)$$

Using Eq. (8), Coles "law of the wake" (log-wake law) takes the form

$$u^+ = \frac{1}{\kappa}\ln y^+ + B + 2\frac{\Pi}{\kappa}\sin^2\left(\frac{\pi}{2}\eta\right) \qquad \ldots \quad (9)$$

Evaluating Eq. (9) at $\eta = 1$ centerline velocity can be obtained

$$U_c{}^+ = U_c / v_* = \frac{1}{\kappa}\ln R^+ + B + 2\frac{\Pi}{\kappa} \qquad \ldots \quad (10)$$

Subtracting Eq. (9) from Eq. (10), one obtains velocity defect law

$$U_c{}^+ - u^+ = \left[-\frac{1}{\kappa}\ln\frac{y^+}{R^+} + 2\frac{\Pi}{\kappa}\right] - 2\frac{\Pi}{\kappa}\sin^2\left(\frac{\pi}{2}\eta\right) \qquad \ldots \quad (11)$$

The part of Eq. (11) in square bracket is the logarithmic part of the defect law in outer scale, applicable for overlap region. The laws (Eqs. (9) and (11)) are applicable to the whole boundary layer except viscous sub-layer and buffer layer. It can be shown that log-wake law and defect law do not satisfy no-slip condition at the wall and do not meet the requirement of

non-zero velocity gradient at the pipe axis. In spite of these shortcomings, many boundary layer computations are based on these laws. As log-wake law/defect law is a composite law, it is difficult to ascertain the end point of the overlap region or beginning of the outer region. For this reason, Coleman[14] located the beginning of the outer region as the non-dimensional elevation y^+ at which the velocity profile curve deviated by 1% from its logarithmic part alone. However, extent of inner region can be determined if two separate laws, one for inner region and other for outer region, are used to describe the flow. Mazumdar and Mandal[15] showed that structure of turbulence in a pipe flow can be described satisfactorily considering Spalding's law of the wall for inner region and Persen's[16] wake law for the outer region. Persen's formulation has the form

$$u^+ - u_\infty{}^+ = \left(\xi - u_\infty{}^+\right) \exp\left[-\frac{\left(y_0{}^+ - y^+\right)^2}{\alpha^2}\right] \quad \ldots \quad (12)$$

where

$$u \to U_c \quad \text{as} \quad y \to R$$

$$u^+ \to U_c / v_* = U_c{}^+ = \xi \quad \text{as} \quad y^+ \to Rv_* / \nu = R^+ = y_0{}^+ \quad \ldots \quad (13)$$

$u_\infty{}^+ = \text{constant}$ and

$$\frac{1}{\alpha^2} = \frac{\ln\left(\xi - u_\infty{}^+\right) - \ln\left(u_1{}^+ - u_\infty{}^+\right)}{\left(y_0{}^+ - y_1{}^+\right)^2} \quad \ldots \quad (14)$$

Here $(u_1{}^+, y_1{}^+)$ is the point where law of the wall meets the law of the wake. Investigating *MK* data, Mazumdar and Mandal[15] showed that inner region occupied about 16.44% of the total boundary layer and this ratio is independent of Reynolds number.

Many values of Π were proposed by the researchers. Zagarola and Smits[9] arrived at $\Pi = 0.329$ from his pipe flow measurements, whereas *MK* found $\Pi = 0.253$ for pipe flow. Analyzing zero pressure gradient (*ZPG*) flow, Coles found $\Pi \approx 0.55$, whereas Osterlund[16] found $\Pi = 0.691$. Coleman obtained $\Pi = 0.19$; Nezu and Rodi[17] reported a value of $\Pi = 0.20$; Kirkgoz[18] observed a value of $\Pi = 0.1$ and Cardoso et al.[19] observed

$\Pi = -0.077$ in smooth channel flow. Considering the reported values of Π, it can be stated that channel flows have minimum wake amongst the three cases (pipe flow, channel flow and *ZPG* boundary layer) whereas *ZPG* flows over a flat plate have highest wake and pipe flows stand in the intermediate position.

Evaluating Eq. (10) with the values of $\kappa = 0.421$, $B = 5.6$ and $2\Pi/\kappa = 1.2$ as proposed *MK* (these are used althrough the paper unless otherwise mentioned)

$$U_c^+ = 2.375 \ln R^+ + 6.800 \quad \ldots \quad (15)$$

Coefficient of determination, r^2 between Eq. (15) and observed values is determined as 0.998 where the correlation coefficient r has the form

$$r = \frac{\sum x_i y_i - \frac{\sum x_i \sum y_i}{N}}{\sqrt{\sum x_i^2 - \frac{\left(\sum x_i\right)^2}{N}} \sqrt{\sum y_i^2 - \frac{\left(\sum y_i\right)^2}{N}}} \quad \ldots \quad (16)$$

where symbol $\Sigma = \sum_{i=1}^{N}$, $x_i = U_c^+(\text{observed})_i$ and $y_i = U_c^+(\text{calculated})_i$.

However, the variables can be considered interchangeably. Average error in estimation E_{av} is determined using the following relation

$$E_{av} = \frac{\sum |\text{observed} - \text{calculated}|}{N}$$

The average error for combined data (*MK* and *HK*) is determined as ±0.130, whereas average error for *MK* and *HK* data are ±0.081 and ±0.232 respectively. Fig. 6 shows how Eq. (15) correlates experimental results.

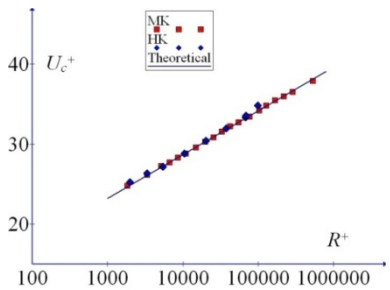

Fig. 6
Centerline velocity and theoretical prediction.

Besides Coles "law of the wake", there are other laws of velocity distributions available in the literature:

Introducing the approximation, $\sin^2\left(\frac{\pi}{2}\eta\right) \approx 3\eta^2 - 2\eta^3$, wake law can be simplified as below (denoted simplified wake law)

Simplified wake law:

$$u^+ = \frac{1}{\kappa}\ln y^+ + B + 2\frac{\Pi}{\kappa}\left(3\eta^2 - 2\eta^3\right) \quad \ldots \quad (17)$$

Lewkowicz[20] :

$$u^+ = \frac{1}{\kappa}\ln y^+ + B + \frac{\Pi}{\kappa}\left\{2\eta^2(3-2\eta) - \frac{1}{\Pi}\eta^2(1-\eta)(1-2\eta)\right\} \quad \ldots \quad (18)$$

Jones[21]:

$$u^+ = \frac{1}{\kappa}\ln y^+ + B - \frac{1}{3\kappa}\eta^3 + \frac{\Pi}{\kappa}2\eta^2(3-2\eta) \quad \ldots \quad (19)$$

Power law :

Main purpose of the present investigation is to use simple power law to depict velocity distribution in a pipe flow. A velocity profile can be empirically expressed as

$$\frac{u}{U_c} = m_1\left(\frac{y}{R}\right)^{\frac{1}{n_1}} = m_1\eta^{\frac{1}{n_1}} \text{ or, } \quad \frac{u^+}{U_c{}^+} = m_1\left(\frac{y^+}{R^+}\right)^{\frac{1}{n_1}} = m_1\eta^{\frac{1}{n_1}} \quad \ldots \quad (20)$$

where m_1 and $1/n_1$ are curve fitting constant and exponent respectively. Time mean velocity u is normalized by centerline velocity of pipe U_c and distance y is normalized by radius of the pipe R. Time mean velocity $u=U_c$ when distance $y = R$. *MK* and *HK* data are plotted in the above scale in Fig. 7.

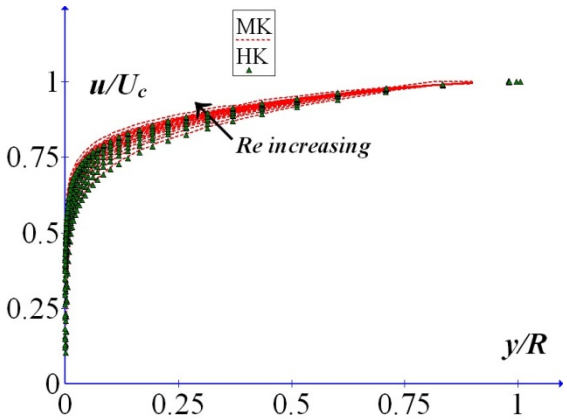

Fig. 7
Variation of mean velocity scaled by centerline velocity.

It is revealed that, the velocity profile becomes more and more uniform as Reynolds number increases. Fig. 7 shows no self similarity but form a family of curves for different Reynolds numbers. Reynolds number dependency of the curve is investigated here using *MK* and *HK* data. Unlike Fig.1, this plot has a definite trend with Reynolds numbers.

Values of m_1 and n_1 are determined using method of least-squares. A brief description of the working principle of the method is given here.

Let us consider data set $x_i = (y/R)_i, y_i = (u/U_c)_i$ and $i = 1, 2, 3, ...N$, where N is number of data points. It is desired to fit $Y = m_1 x^{1/n_1}$ to the data. Straight line form of the equation

$$\ln Y = \ln m_1 + \frac{1}{n_1} \ln x$$

Sum of square of errors

$$E^2 = \Sigma \left(\ln y_i - \ln m_1 - \frac{1}{n_1} \ln x_i \right)^2$$

Values of m_1 and $1/n_1$ are determined by setting $\partial E^2/\partial m_1 = 0$ and $\partial E^2/\partial(1/n_1) = 0$. This procedure leads to

$$\ln m_1 = \frac{\Sigma \ln y_i \Sigma \ln^2 x_i - \Sigma \ln x_i \ln y_i \Sigma \ln x_i}{N\Sigma \ln^2 x_i - (\Sigma \ln x_i)^2}$$

$$\frac{1}{n_1} = \frac{N\Sigma \ln x_i \ln y_i - \Sigma \ln y_i \Sigma \ln x_i}{N\Sigma \ln^2 x_i - (\Sigma \ln x_i)^2}$$

and coefficient of determination

$$r^2 = \frac{\ln m_1 \Sigma \ln y_i + (1/n_1)\Sigma \ln x_i \ln y_i - (\Sigma \ln y_i)^2/N}{\Sigma \ln^2 y_i - (\Sigma \ln y_i)^2/N}$$

where r is correlation coefficient. Values of m_1, $\frac{1}{n_1}$ and r^2 are determined using data of *MK* and *HK*. Variation of m_1 and n_1 are plotted against *Re* in Figs. 8 and 9. Values of r^2 are given in Table 1.

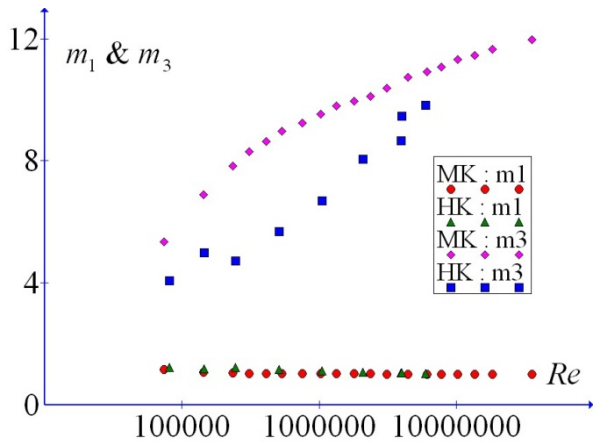

Fig. 8

Variation of curve fitting constants with *Re*.

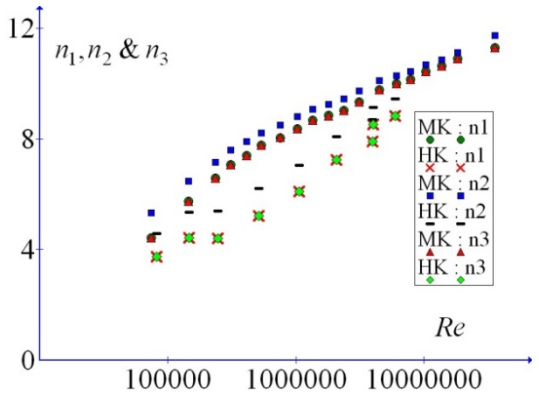

Fig. 9
Variation of n_1, n_2 & n_3 with *Re*.

Table 1
Coefficients of determination for different power laws.

McKeon et al. (2004a) data				Hultmark et al. (2012, 2013)			
Re	r^2(*)	r^2(**)	r^2(***)	Re	r^2(*)	r^2(**)	r^2(***)
7.435E+04	0.890	0.856	0.887	8.133E+04	0.841	0.800	0.841
1.446E+05	0.949	0.934	0.948	1.456E+05	0.859	0.823	0.859
2.340E+05	0.980	0.971	0.979	2.466E+05	0.855	0.813	0.855
3.096E+05	0.991	0.984	0.990	5.125E+05	0.891	0.859	0.891
4.109E+05	0.995	0.990	0.994	1.055E+06	0.909	0.884	0.909
5.369E+05	0.997	0.993	0.996	2.083E+06	0.950	0.936	0.951
7.536E+05	0.997	0.993	0.997	3.951E+06	0.975	0.964	0.975
1.031E+06	0.997	0.993	0.996	4.000E+06	0.991	0.985	0.991
1.346E+06	0.997	0.995	0.997	5.975E+06	0.992	0.986	0.992
1.795E+06	0.997	0.994	0.996				
2.363E+06	0.997	0.994	0.996	(*) Curve : $u/Uc = m_1(y/R)^{1/n1}$			
3.105E+06	0.996	0.994	0.996	(**) Curve: $u/Uc = (y/R)^{1/n2}$			
4.462E+06	0.997	0.995	0.996	(***) Curve: $u^+ = m_3(y^+)^{1/n3}$			
6.113E+06	0.997	0.996	0.997				
7.806E+06	0.998	0.997	0.997				
1.031E+07	0.998	0.997	0.998				
1.372E+07	0.998	0.998	0.998				
1.831E+07	0.999	0.998	0.998				
3.572E+07	0.999	0.997	0.998				

It is revealed that curve fitting constant m_1 is a slowly decreasing function of *Re*. It varies within a small range $1.007 \le m_1 \le 1.231$ with an average value of 1.062. Contrary to m_1, value of n_1 increases as *Re* increases. n_1 ranges between 3.735 to 11.301 with an average 8.660.

As the average value of m_1 is nearly equals to 1, an attempt has been made to derive a similar velocity distribution considering $m_1 = 1$. Modified equation takes the form

$$\frac{u}{U_c} = \left(\frac{y}{R}\right)^{1/n_2} = \eta^{1/n_2} \text{ or, } \quad \frac{u^+}{U_c{}^+} = \left(\frac{y^+}{R^+}\right)^{1/n_2} = \eta^{1/n_2} \qquad \ldots \quad (21)$$

Similar analysis (least square method as done earlier case) is done to determine values of n_2 (using *MK* and *HK* data) which lead to

$$\frac{1}{n_2} = \frac{\sum \ln y_i \ln x_i}{\sum \ln^2 x_i}$$

and coefficient of determination

$$r^2 = \frac{(1/n_2)\sum \ln x_i \ln y_i - \left(\sum \ln y_i\right)^2 / N}{\sum \ln^2 y_i - \left(\sum \ln y_i\right)^2 / N}$$

Values of n_2 are plotted against *Re* in Fig. 8 and r^2 are given in Table 1. Eq. (20) can be re-arranged as

$$u^+ = m_1 \frac{U_c{}^+}{\left(R^+\right)^{1/n_1}} \left(y^+\right)^{1/n_1} = k\left(y^+\right)^{1/n_1}$$

where $k = m_1 \dfrac{U_c{}^+}{\left(R^+\right)^{1/n_1}}$

Attempt has been made to fit the similar equation as above to the data but the equation is considered in its general form

$$u^+ = m_3\left(y^+\right)^{1/n_3} \qquad \ldots \quad (22)$$

where new constant $m_3 \neq k$ and $n_3 \neq n_1$.Values of m_3, n_3 and correlation coefficient, r are determined and those are depicted in Figs. 8, 9 and in Table 1 respectively. It is observed that value of m_3 is increased with *Re*, but values of n_3 is very close to n_1, average deviation $\sum\sqrt{(n_1 - n_3)^2} / N = \pm 0.002$. Correlation coefficient for two cases curve fittings are also very close to each other.

Average velocity :

Average velocity in a pipe may be defined in terms of radial co-ordinate r or wall co-ordinate y, where $y = R - r$ and $dy = -dr$. The distance 'y' is measured from the wall while 'r' is measured from the center of the pipe.

$$V = \frac{1}{\pi R^2}\int_0^R u.2\pi r dr = \frac{2}{R}\int_0^R u dy - \frac{2}{R^2}\int_0^R uy dy$$

Introducing inner variables $u^+ = u/v_*$, $y^+ = yv_*/\nu$ and $R^+ = Rv_*/\nu$

$$V = \frac{2v_*}{R^+}\int_0^{R^+} u^+ dy^+ - \frac{2v_*}{R^{+2}}\int_0^{R^+} u^+ y^+ dy^+ \qquad \ldots \quad (23)$$

Consequently

$$Re = \frac{2VR}{\nu} = 4\int_0^{R^+} u^+ dy^+ - \frac{4}{R^+}\int_0^{R^+} u^+ y^+ dy^+ \qquad \ldots \quad (24)$$

Substituting Coles log-wake law in Eq. (23) one obtains

$$V = v_*\left[\frac{1}{\kappa}\ln R^+ + B + \frac{\Pi}{\kappa} - \frac{3}{2\kappa} - \frac{4\Pi}{\kappa\pi^2}\right]$$

$$V^+ = V/v_* = \frac{1}{\kappa}\ln R^+ + B + \frac{\Pi}{\kappa} - \frac{3}{2\kappa} - \frac{4\Pi}{\kappa\pi^2} \qquad \ldots \quad (25)$$

Considering $\kappa = 0.421$, $B = 5.6$ and $2\Pi/\kappa = 1.20$

$$V^+ = V/v_* = 2.375\ln R^+ + 2.394 \qquad \ldots \quad (26)$$

Eq. (26) is plotted in Fig. 10. It is observed that through the Eq. (26), average velocity can be predicted with r^2 = 0.998 and average error $E_{av} = \pm 0.161$. The average errors are different for two sets of data. For *MK* data and *HK* data E_{av} are ± 0.137 and ± 0.214 respectively. If wake is neglected, V^+ can be approximated as $V^+ = 2.375 \ln R^+ + 2.037$.

It can be shown easily that the relation $V^+ = 2.375 \ln R^+ + 2.037$ will produce same correlation with the data as in case of Eq. (26). However, average error will be different. Average error E_{av} is determined as ± 0.516 which is higher than that in case of Eq. (26).

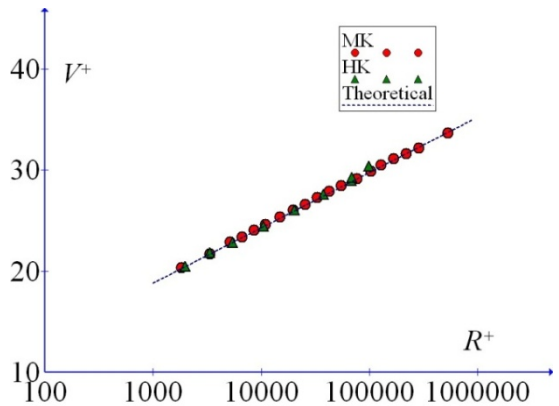

Fig. 10
Analytical estimate of average velocity compared with data**.**

Introducing dimensionless centerline velocity in Eq. (25), average velocity turns out

$$V^+ = U_c{}^+ - \frac{\Pi}{\kappa} - \frac{3}{2\kappa} - \frac{4\Pi}{\kappa\pi^2} \quad \ldots \quad (27)$$

Consequently

$$U_c{}^+ - V^+ = \frac{3}{2\kappa} + \frac{\Pi}{\kappa} + \frac{4\Pi}{\kappa\pi^2} \quad \ldots \quad (28a)$$

and considering $\kappa = 0.421$ and $2\Pi/\kappa = 1.20$, the quantity

$$U_c{}^+ - V^+ = 4.406 \quad \ldots \quad (28b)$$

It is evident beyond doubt that in a turbulent pipe flow, the quantity $\left(U_c^+ - V^+\right)$ has a constant numerical value.

If wake is neglected (only logarithmic law is considered), that is, $\Pi = 0$, the Eq. (28*a*) reduces to

$$U_c^+ - V^+ = \frac{3}{2\kappa} \quad \ldots \quad (29)$$

For the experimental data of Nikuradse[6], *MK*, and *HK* values of $\left(U_c^+ - V^+\right) = 4.07,\ 4.314$ and 4.416 respectively. Considering $\kappa = 0.421$, Eq. (29) gives $\left(U_c^+ - V^+\right) = 3.563$.

Theoretical expression for average velocity will be different from Eq. (25) if other velocity distribution is considered. Some other expressions for average velocity are given below:

Simplified wake law:

$$V^+ = \frac{1}{\kappa}\ln R^+ + B + \frac{3}{5}\frac{\Pi}{\kappa} - \frac{3}{2\kappa} = 2.375\ln R^+ + 2.397 \quad \ldots \quad (30a)$$

$$U_c^+ - V^+ = 4.403 \quad \ldots \quad (30b)$$

Lewkowicz[20] :

same as V^+ obtained from simplified wake law

Jones[21] :

$$V^+ = \frac{1}{\kappa}\ln R^+ + B + \frac{3}{5}\frac{\Pi}{\kappa} - \frac{23}{15\kappa} = 2.375\ln R^+ + 2.318 \quad \ldots \quad (31a)$$

$$U_c^+ - V^+ = 3.690 \quad \ldots \quad (31b)$$

It can be shown easily that the ratio V^+ / U_c^+ is not a constant quantity. The ratio V^+ / U_c^+ can be written as

$$\frac{V^+}{U_c{}^+} = \frac{U_c{}^+ - U_c{}^+ + V^+}{U_c{}^+} = 1 - \frac{U_c{}^+ - V^+}{U_c{}^+} = 1 - \frac{\text{constant}}{U_c{}^+} \quad \ldots \quad (32)$$

Substituting Eq. (15) and Eq. (28b) in Eq. (32)

$$\frac{V^+}{U_c{}^+} = 1 - \frac{4.406}{2.375 \ln R^+ + 6.800} \quad \ldots \quad (33)$$

Constants appearing in the above equation depend on choice of velocity distribution law and value of κ, B and Π. Fig. 11 shows the variation of observed quantity, $V^+ / U_c{}^+$ against R^+. The ratio, $V^+ / U_c{}^+$ is a slowly increasing function of R^+. It ranges between 0.811 to 0.889 with an average of 0.858. Eq. (33) is also potted in Fig. 11 for comparison. It is observed that Eq. (33) is a good approximation of the quantity, $V^+ / U_c{}^+$.

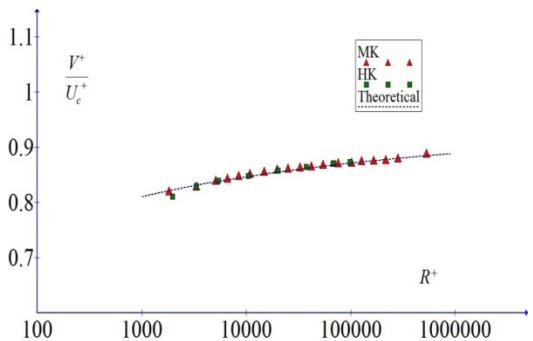

Fig. 11
Variation of the quantity, $V^+ / U_c{}^+$.

Substituting Eq. (20) in Eq. (23)

$$\frac{V}{U_c} = \frac{V^+}{U_c{}^+} = \frac{2 m_1 n_1{}^2}{(1+n_1)(1+2n_1)} \quad \ldots \quad (34)$$

The ratio $V^+ / U_c{}^+$ can be determined from the knowledge of m_1 and n_1. Variation of n_1 obtained from two set of data, are such that it is very difficult to express it in a functional form (Fig.9).

Considering power law $u/U_c = (y/R)^{1/n_2}$

$$\frac{V}{U_c} = \frac{V^+}{U_c{}^+} = \frac{2n_2{}^2}{(1+n_2)(1+2n_2)} \quad \ldots \quad (35)$$

Like n_1, variation of n_2 obtained from two set of data are such that it is very difficult to express it in a functional form (Fig.9).

Location of velocity equals to the average velocity :

Position of the velocity equals to the average velocity can be determined equating u^+ to V^+ and solving the resultant equation. Considering the Coles log-wake law and value of κ and Π as per *MK*, the position

$$\eta = y/R = y^+/R^+ = 0.2419$$

Similarly the positions can be determined considering other velocity distribution. For simplified wake law $\eta = 0.2411$ while it is same as $\eta = 0.2411$ for Lewkowicz[20] law and for Jones [21] law $\eta = 0.2350$.

Friction factor :

Darcy-Weisbach friction factor for smooth pipe can be written as

$$f = \frac{-(dp/dx)D}{\frac{1}{2}\rho V^2} = 8\left(\frac{v_*}{V}\right)^2 = \frac{8}{V^{+^2}} \quad \ldots \quad (36a)$$

$$f = \frac{8gR_H S}{V^2} = 8\frac{v_*{}^2}{V^2} = 4\frac{\rho v_*{}^2}{\frac{1}{2}\rho V^2} = 4\frac{\tau_w}{\frac{1}{2}\rho V^2} = 4C_f \quad \ldots \quad (36b)$$

$$f = 8\frac{v_*{}^2}{V^2} = 32\frac{R^2 v_*{}^2/\nu^2}{4V^2R^2/\nu^2} = 32\frac{(Rv_*/\nu)^2}{(2VR/\nu)^2} = 32\left(\frac{R^+}{Re}\right)^2 \quad \ldots \quad (36c)$$

where dp/dx is the pressure drop per unit length, g is gravitational constant for acceleration, S is slope, shear velocity $v_* = \sqrt{gR_H S} = \sqrt{\tau_w/\rho}$, τ_w is shear stress at the wall and C_f is coefficient of skin friction, the pipe

diameter $D = 2R$, hydraulic radius $R_H = A/P$, A is cross sectional area and P is wetted perimeter.

$Re = 2RV/\nu$ can be obtained substituting expression for u^+ in Eq. (24) or it can be obtained from the derived relation for average velocity V. Consequently, from Eq. (36) friction factor can be obtained. This is to note that different profiles will lead to different expressions for friction factor.

Considering log-wake law, Eq. (9) and using Eq. (24) and Eq. (36) friction factor can be computed as

$$\sqrt{\frac{1}{f}} = \frac{1}{\sqrt{8}}\left[\frac{1}{\kappa}\left(\ln Re\sqrt{f} - \ln\sqrt{32}\right) + B + \frac{\Pi}{\kappa} - \frac{3}{2\kappa} - \frac{4\Pi}{\kappa\pi^2}\right] \quad \text{... (37}a\text{)}$$

substituting the value of κ, B, and $2\Pi/\kappa$ as per *MK*

$$\sqrt{\frac{1}{f}} = 1.934\log\left(Re\sqrt{f}\right) - 0.609, r^2 = 0.99890 \quad \text{... (37}b\text{)}$$

Equation (37*b*) is compared with the data of *MK*, *HK* and Swanson et al.[22] (denoted *SN*) (*SN* data tabulated in McKeon et al.[23]). Coefficient of determination is noted at the right side of the equation.

If wake is neglected $(\Pi = 0)$, the Eq. (37*b*) reduces to

$$\sqrt{\frac{1}{f}} = 1.934\ \log\left(Re\sqrt{f}\right) - 0.735, r^2 = 0.99896 \quad \text{... (38)}$$

Prandtl considered logarithmic law (without wake) with $\kappa = 0.41$ and $B = 5$ and obtained the relation

$$\sqrt{\frac{1}{f}} = 1.99\ \log\left(Re\sqrt{f}\right) - 1.02 \quad \text{... (39)}$$

Equation (39) produces high correlation with data of *MK* and *HK*, $r^2 = 0.99894$.

Prandtl adjusted his theoretical equation with the help of the experimental data of Nikudarse. The adjusted equation is given below with correlation to the data of *MK* and *HK*

$$\sqrt{\frac{1}{f}} = 2.0 \log\left(Re\sqrt{f}\right) - 0.8, r^2 = 0.99898 \quad \ldots \quad (40)$$

Similarly the friction factors *f* are obtained from other laws (using constants as per *MK*)

Simplified log-wake law:

$$\sqrt{\frac{1}{f}} = \frac{1}{\sqrt{8}}\left[\frac{1}{\kappa}\ln\left(Re\sqrt{f} - \ln\sqrt{32}\right) + B + \frac{3}{5}\frac{\Pi}{\kappa} - \frac{3}{2\kappa}\right] \quad \ldots \quad (41a)$$

$$\sqrt{\frac{1}{f}} = 1.934\log\left(Re\sqrt{f}\right) - 0.608, r^2 = 0.99890 \quad \ldots \quad (41b)$$

Lewkowicz[20] law : same as simplified log-wake law

Jones[21] wake law:

$$\sqrt{\frac{1}{f}} = \frac{1}{\sqrt{8}}\left[\frac{1}{\kappa}\ln\left(Re\sqrt{f} - \ln\sqrt{32}\right) + B + \frac{3}{5}\frac{\Pi}{\kappa} - \frac{23}{15\kappa}\right] \quad \ldots \quad (42a)$$

$$\sqrt{\frac{1}{f}} = 1.934\log\left(Re\sqrt{f}\right) - 0.636, r^2 = 0.99891 \quad \ldots \quad (42b)$$

It is revealed from the above that theoretical deduction (39) considering logarithmic law only gives high correlation with the data though is logarithmic law is not a good approximation of velocity profile in comparison to different log-wake laws. It can be explained in this way that logarithmic law overestimates velocity profiles at viscous region and underestimates velocity profile at the outer region and in the process of determining of average velocity, effect of overestimation of velocity at viscous region is neutralized to some extent by the effect of under estimation velocity at the outer region. This is the probable reason of high correlation.

Friction factor considering viscous correction :

Integration of the log-wake law overestimates the average velocity because log-wake law overestimates velocity at viscous region. Consequently, there must be some contribution of this excess average velocity to friction factor. McKeon, et al.[24] proposed addition of the following viscous correction to friction factor relation

$$C = -\frac{19.9}{\left(Re\sqrt{f}\right)^{0.55}}$$

Combining Eq. (37*b*) and viscous correction

$$\sqrt{\frac{1}{f}} = 1.934\log\left(Re\sqrt{f}\right) - 0.609 - \frac{19.9}{\left(Re\sqrt{f}\right)^{0.55}}, r^2 = 0.99874 \qquad \ldots \quad (43)$$

There is high correlation between Eq. (43) the data of *MK* and *HK*. r^2 is given at the right side of the equation. Viscous correction does not improve the relation. It lowers coefficient of determination slightly. Two theoretical relations are compared with data of *MK*, *HK* and *SN* in Fig. 12. At higher Reynolds Number, two relations coincide each other.

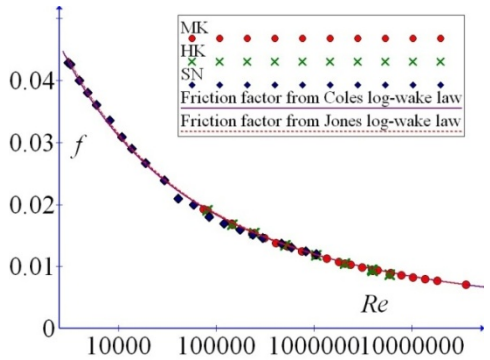

Fig. 12
Theoretical friction factor relations compared with experimental data.

Relation between centerline velocity and friction :

Analyzing *MK* data, Mazumdar and Mandal[15] established relation between U_c^+ and R^+ as $U_c^+ = 2.345 \ln R^+ + 7.157$, $r^2 = 0.9995$.

Considering both *MK* and *HK* data, the relation between U_c^+ and R^+ has the form

$$U_c^+ = 2.352 \ln R^+ + 7.130, \; r^2 = 0.9978 \qquad \ldots \quad (44)$$

Coles law, Simplified law, and Lewkowicz law lead to Eq. (15) for centerline velocity. Centerline velocity obtained from Jones law

$$U_c^+ = \frac{1}{\kappa} \ln R^+ + B - \frac{1}{3\kappa} + 2\frac{\Pi}{\kappa} = 2.375 \ln R^+ + 6.077 \qquad \ldots \quad (45)$$

It is observed that Eq. (15) is very close to Eq. (44) while Equation (45) underestimates the centerline velocity.

As the centerline velocity U_c^+ is a function of R^+ and $R^+ = Re\sqrt{f/32}$, the centerline velocity can be related to friction factor. One obtains from Eq. 15 (which is based on Coles log-wake law)

$$U_c^+ = 5.469 \log\left(Re\sqrt{f}\right) + 2.684 \qquad \ldots \quad (46)$$

The following relation is obtained using Eq. (45) which is based on Jones law:

$$U_c^+ = 5.469 \log\left(Re\sqrt{f}\right) + 1.892 \qquad \ldots \quad (47)$$

The two relations are compared with data in Fig. 13. It can be seen from the Fig. 13 that theoretical relation between centre line velocity and friction factor obtained from Jones[21] law underestimate the experimental data. It is due to underestimation of centerline velocity by the Jones law[21].

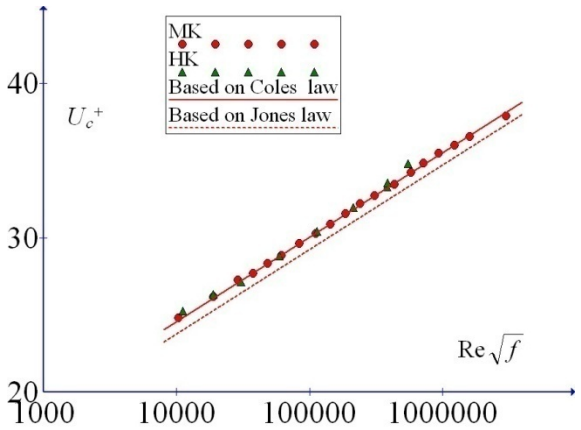

Fig. 13
Theoretical relation $\left(U_c^+ \text{ vs. } Re\sqrt{f}\right)$ compared with data.

Conclusion

All the three power laws produce coefficient of determination greater than 0.9000 for high Reynolds Number. Power law constant m_1 slowly decreases with *Re*. It varies within a small range from 1.01 to 1.23 with an average value of 1.06. The constant n_1 ranges from 3.74 to 11.30 with an average value of 7.89. It increases with *Re*. $n_1 - Re$ relation shows no definite trend. Constant m_3, n_2 and n_3 are increasing function of *Re* but the relations exhibit no definite trend. m_3 ranges between 4.07 and 11.97 with an average value 8.80, average value of n_2 is 8.46 with maximum and minimum value of 11.74 and 4.59 while n_3 ranges between 3.74 to 11.30 with an average value of 7.78.

For turbulent pipe flow, the quantity $\left(U_c^+ - V^+\right)$ has a constant numerical value. Different log-wake laws yield different values of the quantity which ranges from 3.690 to 4.406.

All the theoretical relations for friction factor derived from different log-wake laws give high correlation $\left(\boldsymbol{r}^2 = 0.99890 - 0.99891\right)$ to the data.

Prandtl's adjusted equation gives highest correlation, $r^2 = 0.99898$. It is observed the introduction of viscous correction due to McKeon et al.[24] does not improve friction factor relation. The average velocity is located at non-dimensional height $y / R = y^+ / R^+ = 0.2350$ to 0.2419 from the pipe wall. This can be used to determine average velocity for smooth pipe flow from single measurement.

References

1. McKeon, B. J., Li, J., Jiang, W., Morrison, J.F. and Smits, A.J. – "Further observations on the mean velocity distribution in fully developed pipe flow", J. Fluid Mech., **501,** pp. 135-147 (2004*a*).
2. Schlichting, H. – Boundary-Layer Theory, 7th edition, McGraw-Hill, (1979).
3. Hultmark, M., Vallikivi, M., Bailey, S. C. C. and Smits, A. J. – Turbulent pipe flow at extreme Reynolds numbers, Phys. Rev. Lett., **108 (9)**, 094501 (2012).
4. Hultmark, M., Vallikivi, M., Bailey, S. C. C. and Smits, A. J. – Logarithmic scaling of turbulence in smooth and rough-wall pipe flow, J. Fluid Mech., **728,** 376-395 (2013).
5. Prandtl, L.– "Neuereergebnisse der turbulenzforschung". Z. vdi., **77**, pp. 105-114 (1933).
6. Nikuradse, J. – VDI-Forschungsheft, No. 356, Berlin, (1932).
7. Coles, D. E. – "The law of the wake in the turbulent boundary layer," J. Fluid Mech., **1**, pp.191-226 (1956).
8. Coles, D. E. and Hirst, E. A. – "Proceedings computation of turbulent boundary layer", AFSOR-IFP-Stanford Conference, Vol. II, Stanford University, (1968).
9. Zagarola, M. V. and Smits, A. J. – "Mean flow scaling in turbulent pipe flow," J. Fluid Mech., **373**, pp. 33-79 (1998).
10. Österlund, J.M. – "Experimental studies of zero pressure - gradientturbulent boundary layer flow," Ph. D. Thesis, Royal Institute of Technology, Stockholm, Sweden, (1999).
11. Zanoun, E. S., Nagib, H., Durst, F. and Monkewitz, P. – "Higher Reynolds number channel data and their comparison to recent asymptotic theory,"40th AIAA- 1102, Arospace Science Meeting, Reno, (2002).
12. Spalding, D. B. – "A single Formula for the Law of the Wall," Journal of Applied Mechanics, **28,** Ser. E., pp. 455-458 (1961).

13. Hinze, J.O. – "Turbulence", 2nd Ed., McGraw-Hill, (1975).
14. Coleman, N. L. – "Effects of Suspended Sediment on open-channel Velocity Distribution," Journal of Water Resources research, **22**, No. 10, pp. 1377-1384 (1986).
15. Mazumdar, H.P. and Mandal, B. C. – "Fully developed Pipe flow", U.P.B. Sci. Bull Series D, **73**, Iss. 1, pp. 99-110 (2011).
16. Persen, L.N. – "The Turbulent boundary layer and the closure problem", Proc. AGARD Conf. on Turbulent Boundary Layer-Experiments, Theory and Modelling, pp. 17-1 to 17-14 (1974).
17. Nezu, I. and Rodi, W. – "Open-channel flow measurements with a Laser Dopler Anemometer", J. Hydr. Engrg., ASCE, **112(5)**, pp. 335-355 (1986).
18. Kirkgoz, S. – "Turbulent velocity profiles for smooth and rough open-channel flow," J. Hydr. Engrg., ASCE, **115(11)**, pp.1543-1561 (1989).
19. Cardoso, A. H., Graf, W. H. and Gust, G.– "Uniform flow in smooth open-channel", J. Hydr. Res., IAHR, **27(5),** pp. 603-606 (1989).
20. Lewkowicz, A. K. – "An improved universal wake function for turbulent boundary layers and some of its consequences, Z. Flugwiss. Weltraumforsch, **6,** 261-266 (1982).
21. Jones, M. B. – "Evolution and structure of sink-flow turbulent boundary layers," Ph. D. Thesis university of Melbourne, Australia., (1998).
22. Swanson, C. J., Julian, B., Ihas, G. G. and Donnely, R. J.– "Pipe flow measurements over a wide range of Reynolds numbers using liquid helium and various gases," J. Fluid Mech., **461**, pp. 51-60 (2002).
23. McKeon, B. J., Swanson, C. J., Zagarolla, M. V., Donnelley, R. J. and Smits, A. J. – "Friction factor for smooth pipe flow", J. Fluid Mech., **511,** 41-44 (2004*b*).
24. McKeon, B.J., Zagarola, M.V. and Smith, A.J. – "A new friction factor relationship for turbulent pipe flow," J. Fluid Mech., **538,** 429-443 (2005).

INDIAN JOURNAL OF THEORETICAL PHYSICS, VOL. 64, NOS. 1 & 2, 2016

Ground state of a one dimensional generalised alternating superlattice – a study with Hartree Fock Approximation

Jayeeta Chowdhury

Department of Physics, Scottish Church College,
1, Urquhart Square, Kolkata - 70006, India
E-mail: jyt_ch@yahoo.com, jcphys@scottishchurch.ac.in

(Received for publication in April, 2016)

[**Abstract**: In this work, ground state of a generalised alternating one dimensional superlattice has been studied. The changes in the system property with the changes in the values of site potential and on-site Coulomb repulsion are shown. A self consistent Hartree Fock Approximation calculation is done for this purpose. Studying order parameters of the system, possible phase transition points are found out.]

Key Words: Superlattice, Charge ordering, Spin ordering, Phase diagram

1. Introduction

Owing to the tremendous success in developing different types of low dimensional metallic multilayered structures *e.g.* latered *Fe/Cr* structures[1,3], theoretical study of superlattices is of great importance. Some theoretical and experimental works have been done in this field[1–12]. In the present work I have studied the ground state of a half-filled one dimensional superlattice with unit cell size two. Investigating the order parameters for a range of values of Coulomb repulsion energy and site potential, ground state phase diagram of the system has been drawn.

2. The model and the method

We have modelled the superlattice as a modified Hubbard model with two different values of the site potentials $\varepsilon_A, \varepsilon_B$ and the on-site Coulomb repulsion energies U_A, U_B at the adjacent sites. Previous works on this type of models considered either variations in site potentials or variations in Coulomb repulsion energies. Here is the generalised case where wide range of variations of the both are considered. Scale of energy is chosen by setting

t = 1.0. For this study we have used the Hartree Fock Approximations (*HFA*). Though it is an approximation method, it is now well known that in the weak to moderate coupling regime this method works very well[11].

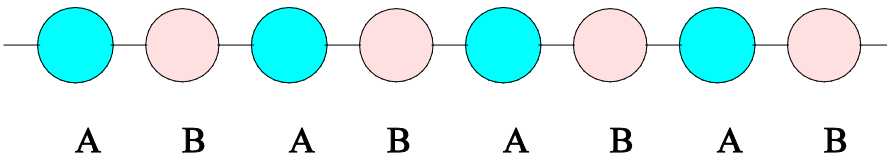

Figure 1

Superlattice chain with two sublattices

The model Hamiltonian is

$$H = \varepsilon_A \sum_{i\in A} n_i + \varepsilon_B \sum_{i\in B} n_i + t\sum_{i,\sigma}(c^{+}_{i,\sigma}c_{i+1,\sigma} + h.c.) + U_A \sum_{i\in A} n_{i\uparrow}n_{i\downarrow} + U_B \sum_{i\in B} n_{i\uparrow}n_{i\downarrow} \quad \ldots \quad (1)$$

U and ε denote on-site Coulomb repulsion energies and site potentials respectively; subscripts indicate the sublattices. In this paper the half-filled band is studied and only the nearest neighbour hopping is considered.

In the Hartree-Fock Approximation, the Coulomb terms is substituted in the following way $(\alpha = A, B)$.

$$U_\alpha n_{i\uparrow}n_{i\downarrow} \to U_\alpha \langle n_{i\uparrow}\rangle n_{i\downarrow} + U_\alpha n_{i\uparrow}\langle n_{i\downarrow}\rangle - U_\alpha \langle n_{i\uparrow}\rangle\langle n_{i\downarrow}\rangle \quad \ldots \quad (2)$$

Now the up and the down-spin terms in the Hamiltonian are decoupled. In an unrestricted *HFA* Hamiltonians can be diagonalised in a self-consistent manner to obtain the single particle energy levels. The ground state is constructed by filling up the energy levels of both the up and the down bands upto the Fermi level.

The ground state properties of these systems can be well-understood from the charge and the spin density order parameters (*c* and *s* respectively). For half-filled chain with periodic boundary condition,

$$c = \frac{1}{2}\left\langle n_{B\uparrow} + n_{B\downarrow} - n_{A\uparrow} - n_{A\downarrow} \right\rangle \quad \ldots \quad (3)$$

$$s = \frac{1}{2}\left\langle n_{B\uparrow} - n_{B\downarrow} - n_{A\uparrow} + n_{A\downarrow} \right\rangle \quad \ldots \quad (4)$$

If '*c*' is greater than '*s*' the system is charge ordered or in other words charge density wave (*CDW*) is formed within the lattice. Otherwise, if '*s*' dominates the system is spin ordered or in other words a spin density wave (*SDW*) is formed.

3. The Result

At first consider the case with $U_A = 2.0$ and $U_B = 0.0$ with $\varepsilon_A = \varepsilon_B = 0.0$ the lattice shows charge ordering[11]. If ε_A is kept fixed at 1.0 it will remain charge ordered, double occupancy at *B* sites being preferred. Now varying ε_B from 0.0 to a high value, it is clearly seen that charge order parameter *c* dominates for all values of ε_B, except 2.0, where spin order parameter dominates (figure 2).

For $U_A = U_B = 2.0$ and zero site potentials, it is a perfect spin ordered phase[11]. If ε_A is changed to 1.0, the lattice is charge ordered. For variation of ε_B from 0.0 to a high value, plots of order parameters (figure 2) show chargeordering for $\varepsilon_B < 0.4$ and $\varepsilon_B > 1.6$. For intermediate values of ε_B the lattice is spin ordered.

Next for the case with $U_A = 2.0$, $U_B = 1.5$, $\varepsilon_B = 1.0$ spin order parameter dominates only for $0.3 < \varepsilon_A < 1.3$ (figure 2). For other values of ε_A the system is charge ordered.

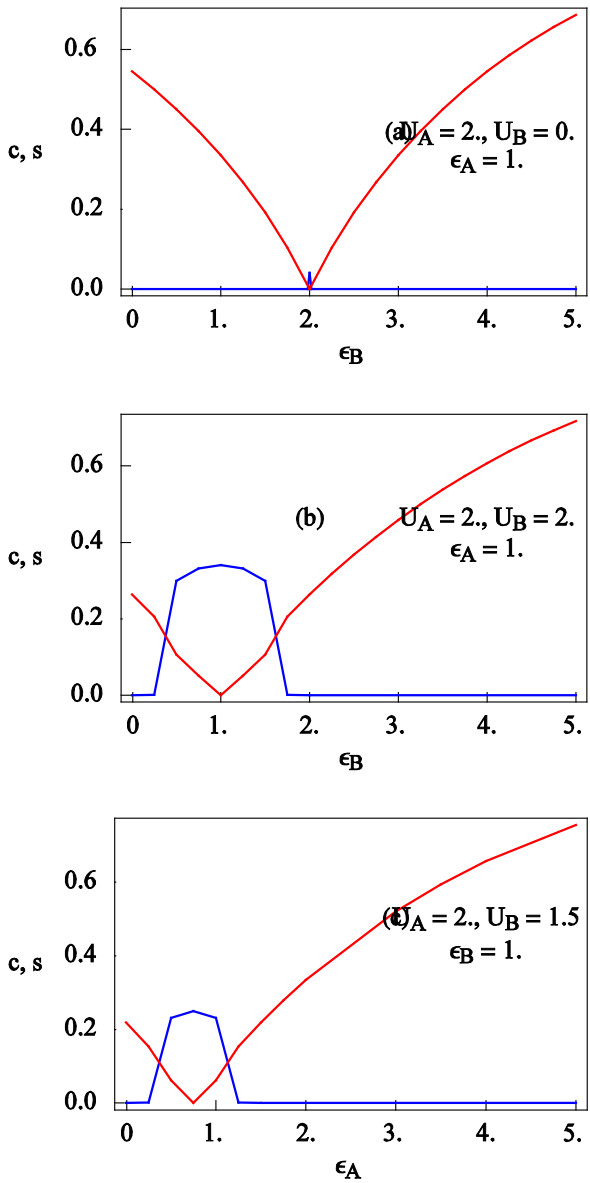

Figure 2

Plots of charge order parameter c (red) and spin order parameter s (blue) with site potentials for $N = 100$. Values of other parameters are shown on diagram. Scale of energy is chosen by setting $t = 1.0$.

Figure 3 shows the variation of order parameters with U_B keeping other parameters fixed. From the plots we can have idea of ordering within the lattice.

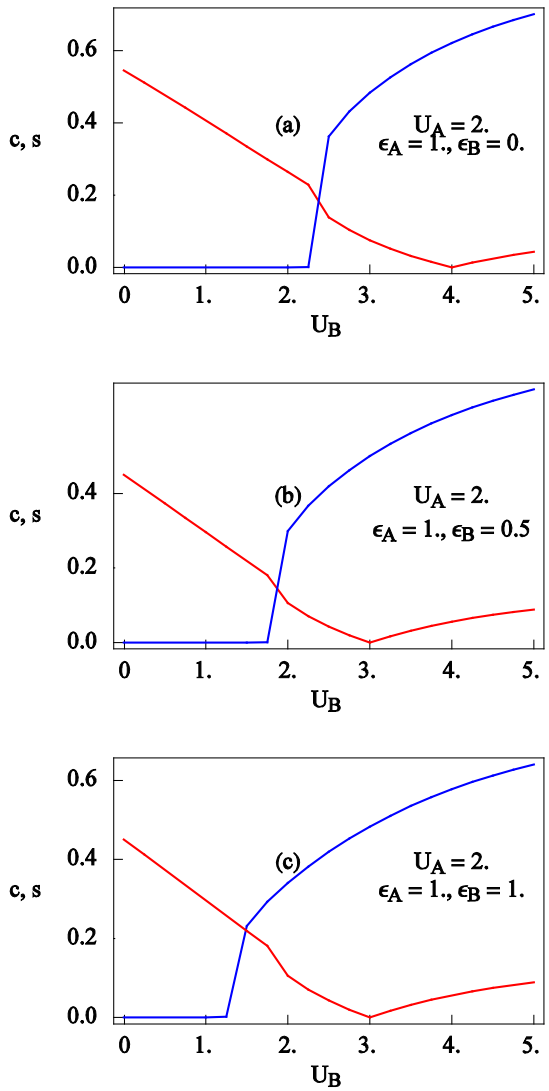

Figure 3

Plots of charge order parameter c (red) and spin order parameter s (blue) with U_B for $N = 100$. Values of other parameters are shown on diagram. Scale of energy is chosen by setting $t = 1.0$.

Having knowledge of the transition points from the order parameter values, phase diagrams for the superlattices are constructed. Various types of phase diagrams are possible. In figure 4, U_B and ε_A are kept fixed. Studying the order parameters with the variations of $U_A(=U)$ and $\varepsilon_B(=\varepsilon)$ regions of charge ordering and spin ordering are located. In the figure 5, U_A and ε_A are kept fixed. $U_B(=U)$ and $\varepsilon_B(=\varepsilon)$ are varied to study the system. Different phases are clear from the diagram.

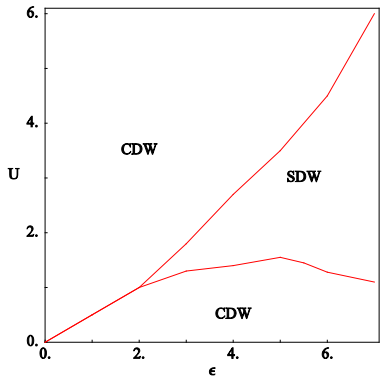

Figure 4

The *HFA* phase diagram in the $U_A(=U)$ – $\varepsilon_B(=\varepsilon)$ plane with $U_B = 0.0$ and $\varepsilon_A = 0.0$ Scale of energy is chosen by setting t = 1.0.

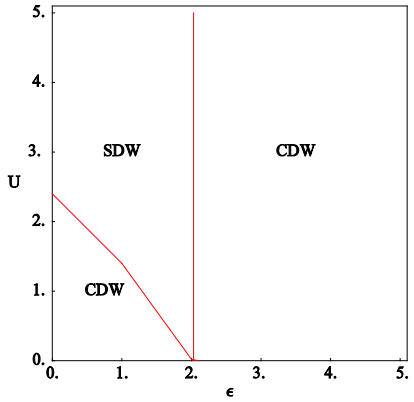

Figure 5

The *HFA* phase diagram in the $U_B(=U)$ – $\varepsilon_B(=\varepsilon)$ plane with $U_A = 2.0$ and $\varepsilon_A = 1.0$ Scale of energy is chosen by setting t = 1.0.

3. Conclusion

Most of the previous works on alternating superlattice models considered a limited ranges of the parameters U_A, U_B, ε_A and ε_B. In this work, many possible combinations of U_A, U_B, ε_A and ε_B have been studied. Convergence of the results with system size has been checked. The phase diagrams show two transition lines, separating a spin ordered region (*SDW*) and two charge ordered regions (*CDW*). This model can be further explored for finite temperatures and for different fillings. Till now there is no experimental work with these wide ranges of variations of the parameters. The results obtained in this work indicate that it would be an interesting experimental study.

References

1. Heinrich, B. and Cochran, J. F. – Adv. Phys., **42**, 523 (1993).
2. Parkin, S. S. P., More, N. and Roche, K. P. – Phys. Rev. Lett., **64**, 2304 (1990).
3. Baibich, M. N., Broto, J. M., Fert, A., Nguyen, Van Dau F., Petroff, F., Etienne, P., Creuzet, G., Friederich, A. and Chazelas, J. – Phys. Rev. Lett., **61**, 2472 (1988).
4. Paiva, T. and dos Santos, R. R. – Phys. Rev. Lett., **76**, 1126 (1996).
5. Paiva, T. and dos Santos, R. R. – Phys. Rev. B, **58**, 9607 (1998).
6. Paiva, T. and dos Santos, R. R. – Phys. Rev. B, **65**, 153101 (2002).
7. Malvezzi, A. L., Paiva, T. and dos Santos, R. R. – Phys. Rev. B, **73**, 193407 (2006).
8. Silva-Valencia, J., Miranda, E. and dos Santos, R. R. – J. Phys.: Condens. Matter, **13**, L609 (2001).
9. Kakashvili, P. and Japaridze, G. I. – J. Phys.: Condens. Matter, **16**, 5815 (2004).
10. Gupta, S., Sil, S. and Bhattacharyya, B. – Phys. Rev. B, **63**, 125113 (2001).
11. Chowdhury, J., Karmakar, S. N. and Bhattacharyya, B. – Phys. Rev. B, **75**, 235117 (2007).
12. Chowdhury, J., Karmakar, S. N. and Bhattacharyya, B. – J. Phys.: Condens. Matter, **21**, 15302 (2009).

INDIAN JOURNAL OF THEORETICAL PHYSICS, VOL. 64, NOS. 1 & 2, 2016

Study of hot-electron effect in thermistors

Rajesh Kumar
University Department of Electronics,
B.R.A. Bihar University, Muzaffarpur-842001, Bihar

and

Tarun Kumar Dey
Post Graduate Department of Physics, L. S. College
Muzaffarpur-842001, Bihar
E-mail : tkdeyphy@gmail.com

(Received for publication in May, 2016)

[**Abstract:** In this paper we study non-ohmic behavior of doped silicon and germanium using a hotelectron model, which is motivated by the hot-electron effect in metals at low temperatures. This model assumes that the thermal coupling between electrons and lattice at low temperatures is weaker than the coupling between electrons, so that the electric power applied to the electrons raises them to a higher temperature than the lattice. Although this model seems not suitable for semiconductors in the variable range-hopping regime, where the electrons are localized, it fits quite well the experimental data. To determine whether the hot-electron model in doped semiconductor is just an alternative way to parameterize the data or has some physical validity, we investigated the noise and the frequency dependence of the impedance of doped silicon thermistors that are used for low temperature thermal *X*-ray detectors. The measured excess white noise at low frequencies is consistent with the predicted thermodynamic fluctuations of energy between electron and phonon systems. The non-ohmic behavior shows a characteristic time that can be interpreted as a *C/G* time constant in the hot-electron model. By measuring this time constant, we get a hot-electron heat capacity *C* that agrees with the measured excess heat capacity of the implants. These support the assumption of a hot-electron system thermally separated from the lattice system.]

1. Introduction

Non-Ohmic effects of ion-implanted silicon thermistors can be well described by the "hot-electron" model[1,9,10], where it is assumed that the resistance depends only on the temperature of the electrons, but there is a thermal resistance between the electrons and the crystal lattice through

which the bias power must flow, increasing the temperature of the electrons above the temperature of the lattice, and therefore reducing the thermistor resistance.

Figure 1 shows the resistance of a thermistor as a function of the Joule power for different phonon (lattice) temperatures ranging from 50 *mK* to 150 *mK*. The lines are the result of a fit to the hot-electron model, with a power-law dependence of thermal conductivity on temperature. The hot-electron model seems to fit very well and the parameters derived are in good agreement with the previous results[1,3,5].

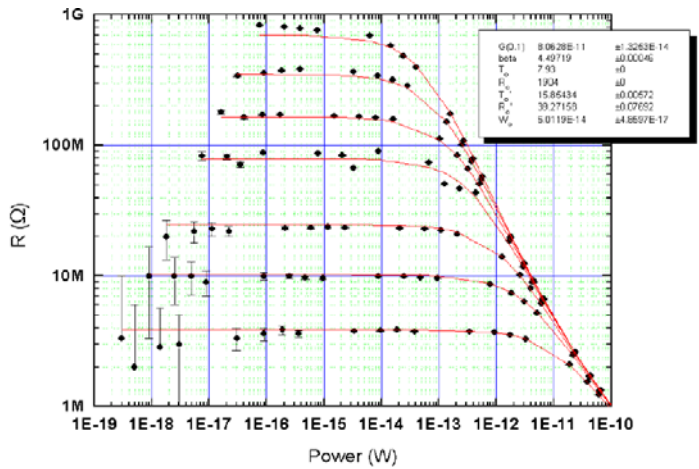

Figure 1

The resistance-vs.-Joule power plot of a silicon thermistor, with the lattice temperature ranging from 50 *mK* to 150 *mK*. Each curve is the result of the fit to the hot-electron model at the corresponding electron temperature.

Hot-electron effects are well-understood in metals[4-8], but in hopping semiconductors the electrons are expected to be localized in the lattice and therefore the theory does not predict any hot-electron behavior. In order to find out whether the hot-electron effect is physical in doped semiconductors, despite the theoretical predictions, we studied other effects that it would generate. The study of the excess noise and the frequency-dependence of the non-linear effects of the silicon thermistors give us more experimental supports to the physical validity of this model. The devices that we tested

have a wide variety of dimensions, with thickness of either about 1.5 μm or 0.3 μm, areas between 2.5×10^{-5} cm^2 and 1.6×10^{-3} cm^2, and geometries between 1×36 and 36×1.

2. Interpreting the excess white noise

The hot-electron model can be used to explain the excess white noise that we measured in implanted silicon thermistors.

During the characterization of thick silicon thermistors, we measured the noise between 3 *Hz* and 30 *kHz* on devices in strong thermal connection with the cold plate of the refrigerator (*i.e*. the devices were not suspended and the chip they were mounted on was glued to the cold plate) under different bias conditions. The phonon noise due to thermal fluctuation between the devices and the heat sink is expected to be negligible due to the strong thermal link. The only appreciable noise contribution expected was Johnson noise, but we found that, for bias currents greater than zero, the devices produce an excess noise. This excess noise is flat at low frequencies and has a roll-off at about 500-5,000 *Hz* due to the stray capacitance of the *FET* readout electronics.

We then tried to explain this excess noise in the context of the hot-electron model. If the electrons and phonons are really two separate systems connected through a thermal conductivity $G_{e\text{-}ph}$, we expect, in addition to the Johnson noise, to see the noise due to thermal fluctuations between the two systems[2,3].

Figure 2 (left) shows the measured excess noise as a function of the expected phonon noise due to the thermal link between electrons and phonons. In the calculations, for the value of the thermal conductivity we used the value obtained from the fit of the resistance-vs.-power plot. The plot shows a strong correlation between the observed excess noise and the expected thermal noise, with a linearly fit with a slope of nearly 1. This strongly supports the idea that the excess noise is due to thermal fluctuations between electrons and phonons, and that the hot electron model may be something more than just a good empirical way to explain the non-ohmic behavior of semiconductor thermistors.

We also considered the possibility that only Johnson noise exists and that the excess noise is due to an underestimate of it. If this were the case, there should be a systematic error apparent in our measurements, and the excess noise should scale with the expected Johnson noise. To make sure that this is not the case, we made a plot of excess noise vs. expected Johnson noise in figure 2 (right). In this plot, the data points are widely scattered, and cannot be reasonably fitted in any way. Therefore, the apparent excess noise doesn't seem to be related in any way to the Johnson noise.

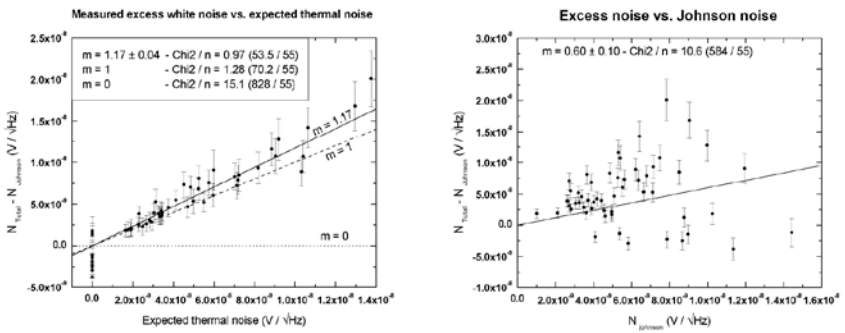

Figure 2

The left figure shows the good fit of the measured excess white noise to the expected thermal noise from the hot-electron model. The data are taken from several deep-implanted samples. The right figure shows that the excess white noise is not linear with the Johnson noise, thus makes sure that it is not due to an underestimate of the Johnson noise.

3. Heat capacity of the hot-electron system

Assuming that the hot-electron model describes a real physical property of silicon thermistors, we considered other effects predicted by this model and tried to experimentally see them. In particular, if the electrons constitute a separate system, we expect them to have a heat capacity C_e greater than zero. This heat capacity combines with the thermal conductivity $G_{e\text{-}ph}$, and should show up as a characteristic time constant in the resistance non-linearity with a value equal to $C_e / G_{e\text{-}ph}$.

We therefore measured the dynamic impedance $Z(w)^2$ of different thermistors under several bias conditions. Since these devices are in strong thermal contact with the heat sink, the time constant between the thermistors

and the heat sink should be zero, and any time constant characterizing *Z(w)* must come from the hot-electron system. Fitting the measured dynamic impedance we obtain, in fact, a time constant $C_e/G_{e\text{-}ph}$ that is different from zero, which implies that there is a heat capacity, or something that behaves like a heat capacity associated with the hot-electron system. Moreover, we estimate the value of the heat capacity C_e using the $G_{e\text{-}ph}$ obtained through the resistance-vs.-power curves.

Figure 3 shows the plot of C_e vs. electron temperature. The data from different thermistors and under different bias conditions seem to be consistent to each other, with a power-law dependence on the temperature that has an index smaller than one.

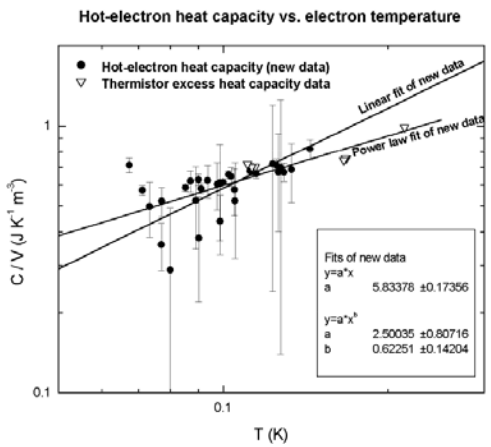

Figure 3

The hot-electron heat capacity obtained from the measured characteristic time *C/G* and the heat conductance *G*. The data show a power-law dependent on the electron temperature and a good agreement with the measured thermistors excess heat capacity.

The error bars are mainly due to stray capacitances in the electrical circuit that limit the accuracy in the measurement of the time constant. The results are in good agreement with the measured total excess heat capacity associated with the thermistor (shown in figure 3). Those values were obtained by taking the difference of the total heat capacity of two detectors that were identical except for an extra thermistor implant on one of them.

References

1. Zhang, J., Cui, W., Juda, M., McCammon, D., Kelley, R. L., Moseley, S. H., Stahle, C. K., and Szymkowiak, A. E. – Phys. Rev., B **57**, 4472-4481 (1998).
2. Mather, J. C., – Appl. Opt., **21**, 1125-1129 (1982).
3. Moseley, S. H., Mather, J. C. and McCammon, D. – J. Appl. Phys., **56**, 1257-1262 (1984).
4. Little, W. A. – Can. J. Phys., **37**, 334-349 (1959).
5. Shklovskij, V. A. – J. Low Temp. Phys., **41**, 375-396 (1980).
6. Anderson, A. C. and Peterson, R. E. – Phys. Lett., **38A**, 519-520 (1972).
7. Anderson, P. W., Abrahams, E., and Ramakrishnan, T. V. – Phys. Rev. Lett., **43**, 718-720 (1979).
8. Roukes, M. L., Freeman, M. R., Germain, R. S., Richardson, R. C. and Ketchen, M. B. – Phys. Rev. Lett., **55**, 422-425 (1985).
9. Wang, X., Sui, Y., Song, X., Zhu, R., Qian, Z., Su, W. and Jinke, T. – J. Applied Phys., **101** (9), p. 09J509 - 09J509-3 (2007).
10. Wan, F., Jalil, M.B.A., Tan, S.G. and Fujita, T. – Journal of Applied Physics, **103** (7), p. 07B731 - 07B731-3 (2008).

INDIAN JOURNAL OF THEORETICAL PHYSICS, VOL. 64, NOS. 1 & 2, 2016

Radiative fluid flow over a non-linearly stretching sheet in porous medium with chemical reaction

Pradip Kumar Gaur, Ram Prakash Sharma*
and
Abhay Kumar Jha

(Received for publication in May, 2016)

[**Abstract:** In this paper the influence of thermal radiation, suction/blowing parameter, and chemical reaction parameter on heat and mass transfer properties past a non linearly stretching sheet subjected to steady 2-*D* magnetohydrodynamic fluid flow through porous medium are studied. The governing 2-*D* boundary-layer partial differential equations are transferred to ordinary differential equations containing radiation parameter, permeable parameter, chemical reaction parameter, suction/blowing parameter, magnetic field parameter, Prandtl number, and Schmidt number. These equations are solved numerically by shooting method with fourth-fifth-order Runge-Kutta integration technique. The effects of the governing parameters on velocity, temperature and concentration are plotted and discussed in details.]

Keywords: Thermal radiation; MHD; Suction/blowing parameter; Chemical reaction; Non-linear stretching surface

1. Introduction

The study of flow and heat transfer induced by a stretched surface is important in many industrial processes *e.g*., in the manufacture and drawing of rubber sheets, plastics, glass-fiber, paper production, metal processes, polymer extrusion processes, crystal growing, cooling of metallic sheets in a cooling bath and many others. Sakiadis[1-3] have studied the boundary-layer behavior on continuous solid surfaces. Gurubka and Bobba[4] have studied heat transfer effects on a continuous stretching surface with variable temperature. Fluid flow past a stretching sheet has been presented by Kumaran and Ramnath[5]. The flow of a fluid past a nonlinearly stretching sheet has studied by Vajravelu[6]. Heat and mass transfer on a stretching sheet

*Corresponding Author Email : ramprakash0808@gmail.com

have analyzed by Elbashbeshy[7]. Vajravelu and Cannon[8] have studied the flow of fluid past a nonlinearly stretching sheet. An analysis of viscous flow and heat transfer on a nonlinearly stretching surface in the presence of various parameters has been presented by Coretell[9-11]. Hayat, et al.[12] have studied mixed convection flow on a nonlinearly stretching sheet. An *MHD* flow past a nonlinear stretching sheet has been studied by Hayat, et al.[13]. The fluid flow and heat transfer past a non-linearly stretching surface has been investigated by Cortell[14]. Shahzad and Khan[15] have presented an exact solution for the radiative flow and heat transfer past a nonlinear stretching sheet. Mukhopadhyay[16] have presented a study of a boundary layer flow past a nonlinearly stretching sheet with partial slip. Ferdows, et al.[17] have studied *MHD* radiative boundary layer natural convection flow and heat mass transfer over a nonlinearly stretching sheet. Rashidi, et. al.[18] have analyzed natural convection heat and mass transfer for *MHD* radiative fluid flow past a vertical stretching sheet with buoyancy effects. Cortell[19] have studied *MHD* radiative visco-elastic fluid flow past a stretching surface in the presence of heat absorption/generation.

The analysis of flow and heat mass transfer with *MHD* has considerable theoretical and practical importance because the boundary layer flow can be controlled by the magnetic field. *MHD* flow has widespread application in the field of engineering, *e.g.*, nuclear reactors, *MHD* generators, polymer technology, metallurgy, and plasma studies etc. The analysis of Magnetohydrodynamic fluid flow in porous medium is of considerable attention in industry and environment. Some of the applications are flow of ground water through soil and rocks (porous medium), extraction of oil and natural gas from rocks, functioning of tissues in body (bone, cartilage, and muscle etc. being porous media) and flow of blood through them, and understanding various medical conditions (such as tumor growth, a formation of porous medium) and their treatment (such as injection, a flow through porous media) in medical science. The analysis of Magnetohydrodynamic fluid flow in porous medium under various conditions have been presented by (Varshney[20]; Vajravelu and Rollins[21]; Afify[22]; Fang, et. al.[23]; Javed, et. al.[24]; Noor et al.[25]; Motsa and Sibanda[26]; Abbasbandy, et. al.[27]; Kumar[28]; Fadzilah, et. al.[29]. Thermal radiation has important applications in the processes involving high temperatures and space technology.

Recently developments in hypersonic flights, space vehicles, gas turbines, nuclear power plants and gas cooled nuclear reactors have attracted researcher in this area. Several researchers investigated thermal radiation as a mode of heat transfer. Cortell[30] have studied thermal boundary flow past a non-linearly stretching surface with radiation and dissipation. Sajid and Hayat[31] have investigated the thermal radiation effect on the boundary layer flow over a stretching surface. An *MHD* radiative natural convective flow has been investigated by Chen[32]. The effects of thermal radiation on fluid flow and heat transfer under various conditions have been presented by (Pal[33]; Ishak, et. al.[34]; Prasad, et. al.[35].

The analysis of heat and mass transfer with chemical reaction is very important due to its applications in engineering and science. The study of mass transfer effects with chemical reaction is useful in chemical processing equipments. Such study is important in electromagnetic propulsion, movement of biological fluids, construction and food engineering, chemical process industries. Chemically reacting fluids have many technological applications ranging from the formation of thin films for, biological systems, combustion reactions, catalysis, and electronics etc. Chamkha[36] have studied *MHD* flow past a stretched vertical sheet with the chemical reaction and heat generation/absorption. Afify[37] have investigated *MHD* free convection flow and mass transfer over a stretching sheet with chemical reaction. The influence of thermophoresis on *MHD* mixed convection heat and mass transfer through a porous wedge with variable viscosity and chemical reaction has been investigated by Kandasamy, et. al[38]. The effect of chemical on heat and mass transfer under various conditions have been presented by (Bhattacharyya and Layek[39]; Rashad and El-Kabeir[40]; Afify and Elgazery[41].

2. Formulation of the problem

Consider a steady, radiative, *MHD* motion of a viscous fluid past a non-linear stretching sheet immersed in a porous medium. The first order chemical reaction is included in the concentration equation, taking the coordinate axes x - and y - along and perpendicular to the sheet respectively. A variable magnetic field $B(x)$ is applied normally to the sheet. In the direction of x - axis the two forces which are equal in magnitude but

opposite in direction are applied, thus the sheet is stretched keeping the origin fixed. We assume that the flow is electrically conducting and the effects of the persuaded magnetic field and electric field are ignored.

Therefore, under such assumptions, governing equations for the flow relevant to the problem are:

$$\frac{\partial u}{\partial x}+\frac{\partial v}{\partial y}=0 \qquad \ldots \quad (1)$$

$$u\frac{\partial u}{\partial x}+v\frac{\partial v}{\partial y}=\upsilon\frac{\partial^2 u}{\partial y^2}-\frac{\sigma B_0^2}{\rho}u-\frac{\upsilon}{K}u \qquad \ldots \quad (2)$$

$$u\frac{\partial T}{\partial x}+v\frac{\partial T}{\partial y}=\frac{k}{\rho Cp}\frac{\partial^2 T}{\partial y^2}-\frac{1}{\rho Cp}\frac{\partial q_r}{\partial y} \qquad \ldots \quad (3)$$

$$u\frac{\partial C}{\partial x}+v\frac{\partial C}{\partial y}=D_m\frac{\partial^2 C}{\partial y^2}-K_c(C-C_\infty) \qquad \ldots \quad (4)$$

The strength of the variable magnetic field $B(x)$ is assumed as $B(x) = B_0 x^{-2/3}$

The relevant boundary conditions are

$$u_w(x)=\frac{\upsilon}{d^{4/3}}x^{1/3}, v=v_w,$$

$$T=T_w(x)=\left(T_\infty+G_1.\left(\frac{x}{d}\right)^{m_3}\right),$$

$$u\to 0, T\to T_\infty, C\to C_\infty \qquad at\ y\to\infty$$

$$C=C_w(x)=\left(C_\infty+H_1.\left(\frac{x}{d}\right)^{m_3}\right)\ at\ \ y=0 \qquad \ldots \quad (5)$$

Rosseland's approximation is used for radiative heat flux which is given below (Cortell[10]):

$$q_r=-\left(\frac{4\sigma^*}{3k^*}\frac{\partial T^4}{\partial y}\right) \qquad \ldots \quad (6)$$

We now introduce the following similarity transformations and dimensionless parameters:

$$\eta = y\frac{x^{-1/3}}{d^{2/3}}, u = \frac{\upsilon}{d^{4/3}}x^{1/3}f'(\eta), \quad v = -\frac{\upsilon}{d^{2/3}}x^{-1/3}\frac{2f-\eta f'}{3}$$

$$\theta(\eta) = \frac{T-T_\infty}{T_w-T_\infty}, \ \varphi(\eta) = \frac{C-C_\infty}{C_w-C_\infty}$$

$$M = \frac{\sigma B_0^2}{\rho\upsilon}d^{4/3} \text{ (Hartmann number)},$$

$$\varsigma = \frac{x^{2/3}d^{4/3}}{K} \text{ (Porosity parameter)},$$

$$\Pr = \frac{\rho C_p \upsilon}{k} \text{ (Prandtl number)},$$

$$\xi = \frac{K_c Sc}{x^{1/3}}d^{4/3} \text{ (Chemical reaction parameter)}$$

$$N_R = \frac{kk^*}{4\sigma^* T_\infty^3} \text{ (Radiation parameter)},$$

$$Sc = \frac{\upsilon}{D_m} \text{ (Schmidt number)},$$

$$k_2 = \frac{3N_R}{3N_R+4} \text{ (Constant)} \qquad \ldots \quad (7)$$

Now using equation (6) and (7) the mass conservation equation (1) is identically satisfied, and substituting into equation (2), (3) and (4), we get

$$3f''' + 2ff'' - (f')^2 - 3(M+\varsigma)f' = 0 \qquad \ldots \quad (8)$$

$$\theta'' + \Pr k_2\left(\frac{2}{3}f\theta' - m_3 f'\theta\right) = 0 \qquad \ldots \quad (9)$$

$$\varphi'' + Sc\left(\frac{2}{3}f\varphi' - m_3 f'\varphi\right) - \xi\varphi = 0 \qquad \ldots \quad (10)$$

By considering $m_3 = 0$, $G_1 = T_w - T_\infty$ and $H_1 = C_w - C_\infty$ the boundary conditions[5] become

$$f = -S, f' = 1, \theta = 1, \varphi = 1 \ \ at \ \eta = 0$$

$$f' \to 0, \ \theta \to 0, \ \varphi \to 0 \ \ at \ \eta \to \infty \qquad \ldots \quad (11)$$

where $a = v_w \dfrac{3d^{2/3}}{2v} x^{1/3}$ (suction/blowing parameter).

3.Numerical solutions

The equations (8), (9) and (10) are solved numerically with the boundary conditions (11) by applying 4th order Runge-Kutta method along with shooting technique. We first reduce the equations (8), (9) and (10), into first order differential equations, by using

$$S_1 = f, S_2 = f', S_3 = f'', S_4 = \theta, S_5 = \theta', S_6 = \varphi, S_7 = \varphi'.$$

Thus we get

$$S_1' = S_2$$

$$S_2' = S_3$$

$$S_3' = (M + \varsigma) S_2 - \frac{2}{3} S_1 S_3 + \frac{1}{3} S_2^2$$

$$S_4' = S_5$$

$$S_5' = \left[\Pr k_2 \left(m_3 \, S_2 \, S_4 - \frac{2}{3} S_1 S_5 \right) \right]$$

$$S_6' = S_7$$

$$S_7' = \xi \, x_6 - Sc \left(\frac{2}{3} S_1 S_7 - m_3 \, S_2 S_6 \right) \qquad \ldots \quad (12)$$

Subject to the following initial conditions

$$S_1 = -S, S_2 = 1, S_3 = u_1, S_4 = 1, S_5 = u_1, S_6 = 1, S_7 = u_3 \qquad \ldots \quad (13)$$

The equations (12) and (13) solved numerically by utilizing 4th order Runge-Kutta method along with shooting technique. In equation (13) u_1 , u_2 and u_3 are unidentified to be resolute as the part of numerical solution and the results are illustrated numerically and graphically.

From the equations (7) and (11) the shearing stress at the stretched surface is derived below:

$$\tau_w = \mu\left(\frac{\partial u}{\partial y}\right)_w = \mu\frac{\upsilon}{d^2}f''(0) \quad \text{... (14)}$$

From the equations (6) and (11) the heat flux in expressions of Nusselt number at the surface is derived below :

$$q_w = -k\left(\frac{\partial T}{\partial y}\right)_{y=0} + (q_r)_w = -\frac{kG}{k_2 d}\theta'(0)\left(\frac{x}{d}\right)^{m_3 - 1/3} \quad \text{... (15)}$$

If $m_3 = -2/3$, then equation (15), reduces to

$$q_w = -\frac{kG_1}{k_2 d}\theta'(0) \quad \text{... (16)}$$

The nusselt number is given by

$$Nu_x = \frac{xq_w}{k\left(T_w(x) - T_\infty\right)} \quad \text{... (17)}$$

From Eq. (11), (16) and (17), we obtain

$$Nu_x = \frac{-\theta'(0)}{k_2}\left(\frac{x}{d}\right)^{2/3} \quad \text{... (18)}$$

The local Reynolds number can be obtained as

$$\mathrm{Re}_x = u_w(x)\frac{x}{\upsilon} = \left(\frac{x}{d}\right)^{4/3} \quad \text{... (19)}$$

From equations (18) and (19), we obtain

$$Nu_x . \mathrm{Re}_x^{-\frac{1}{2}} = -\frac{\theta'(0)}{k_2} \quad \text{... (20)}$$

From the equations (6) and (11), the mass flux in expressions of Sherwood number is derived below:

$$M_w = -D_m\left(\frac{\partial C}{\partial y}\right)_{y=0} = -D_m H\frac{\varphi'(0)}{d}\left(\frac{x}{d}\right)^{m_3 - \frac{1}{3}} \quad \text{... (21)}$$

If $m_3 = -2/3$, then equation (21), reduces to

$$M_w = -D_m H_1 \frac{1}{x} \varphi'(0) \quad \text{... (22)}$$

The Sherwood number can be obtained as

$$Sh = \frac{x M_w}{D_m \left(C_w(x) - C_\infty\right)} \quad \text{... (23)}$$

From equations (11), (21) and (23), we obtain

$$Sh = \varphi'(0) \left(\frac{x}{d}\right)^{2/3} \quad \text{... (24)}$$

The local Reynolds number can be obtained as

$$\mathrm{Re}_x = u_w(x) \frac{x}{\upsilon} = \left(\frac{x}{d}\right)^{4/3} \quad \text{... (25)}$$

From the equations (24) and (25), we get

$$Sh.\mathrm{Re}_x^{-\frac{1}{2}} = -\varphi'(0) \quad \text{... (26)}$$

4. Results and Discussion

In order to study the nature of the velocity, heat and mass transfer, shear stress and rate of heat and mass transfer, numerical calculations are carried out for distinct values of $M, \varsigma, \mathrm{Pr}, N_R, a, m_3, \xi$ and *Sc* which are listed in figures and the results are reported graphically.

Figures 1 to 3 illustrate the influences of the Hartmann number, porosity parameter and blowing/suction parameter on the fluid velocity. We observe that velocity decelerate with the growing value of porosity parameter, Hartmann number and suction parameter while it enhances as blowing parameter increases because the presence of M, ς and $a(<0)$ decelerate the thickness of the momentum boundary layer while it is enhanced in the case of blowing parameter. The influences of the Hartmann number, porosity parameter and blowing/suction parameter on the temperature profile are shown in figures 4 to 6. We observe that temperature enhances with the growing value of blowing parameter while the reverse trend is seen for

Hartmann number, porosity parameter and suction parameter because the presence of M, ς and $a(<0)$ decelerate the thickness of the thermal boundary layer while it is enhanced in the case of blowing parameter.

Figures 7 and 8 shows the effects of radiation parameter and blowing/suction parameter on the temperature at $m_3 = 0$. We observe that, when the value of the wall temperature parameter is zero, the occurrence of radiation parameter increases the temperature profiles. Furthermore, in the case of blowing parameter ($a = 0.5$), we found significant differences in temperature profile. Figure 9 presented the effects of radiation parameter and wall temperature parameter on the temperature profile at $a = 0$ (impermeable surface). We noticed that the temperature profile diminish with the increasing value of radiation parameter. Furthermore, the temperature profiles decreases with the growing value of wall temperature parameter. The reason is that the radiation parameter and wall temperature parameter depress the thickness of the thermal boundary layer. The influences of Schmidt number and chemical reaction parameter on the concentration profile presented in figures 10 and 11. We noticed that the concentration profile depress with the growing value of Schmidt number and chemical reaction parameter. From figure 12 it is noticed that the magnitude of $f''(0)$ being larger for the growing value of blowing parameter while opposite trend is found for the suction parameter. From figures 13 and 14 it is noticed that the magnitude of $-\theta'(0)$ is larger for the growing value of radiation parameter and wall temperature parameter. The magnitude of is higher for the growing value of the wall temperature parameter as seen in figure 15.

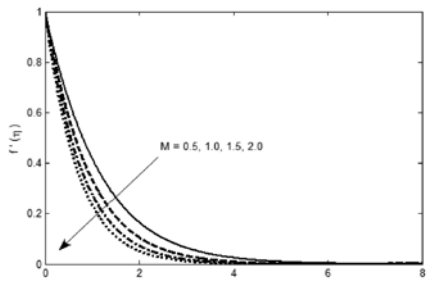

Figure 1
Velocity profiles for various Hartmann number.

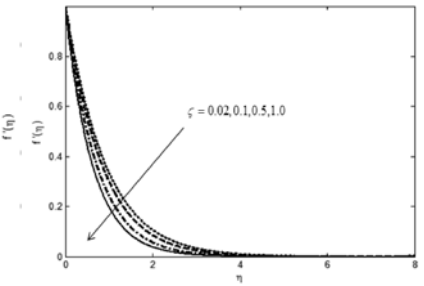

Figure 2
Velocity profiles for various values of porosity parameter.

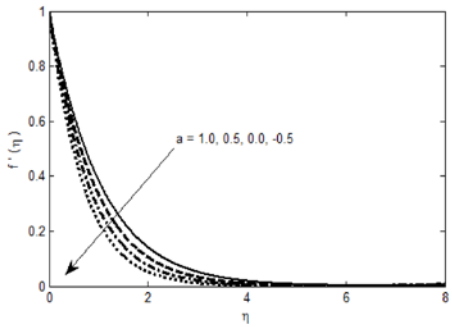

Figure 3
Velocity profiles for various values of blowing/suction parameter.

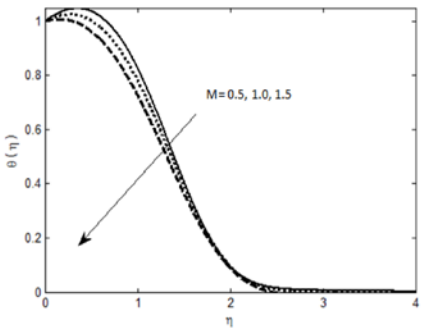

Figure 4
Temperature profiles for various values of Hartmann number.

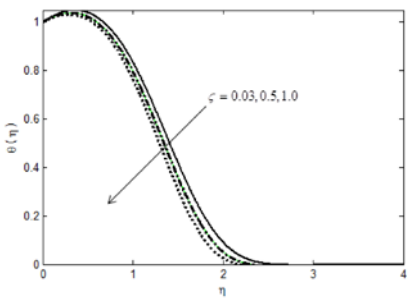

Figure 5
Temperature profiles for various values of porosity parameter.

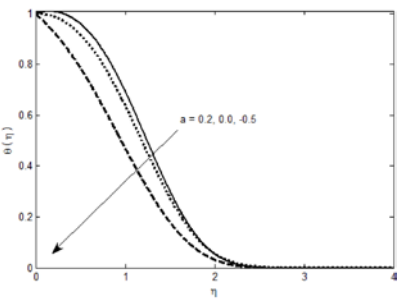

Figure 6
Temperature profiles for various values of blowing/suction parameter.

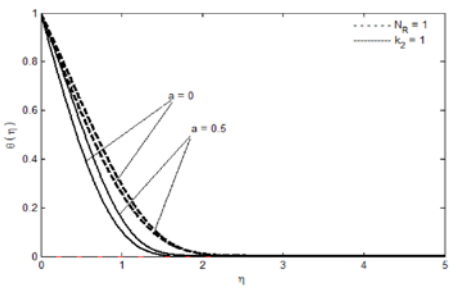

Figure 7
Temperature profiles for radiation Parameter and blowing parameter when m_3=0 and with (n_r =1) and without (k_2=1) radiation effect.

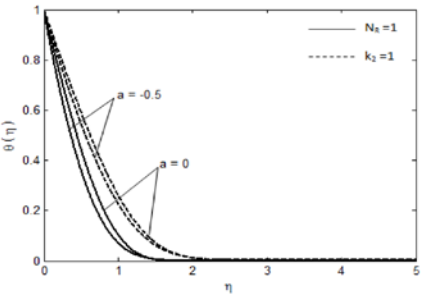

Figure 8
Temperature profiles for radiation parameter and suction parameter when m_3=0 and with (n_r =1) and without (k_2=1) radiation effect.

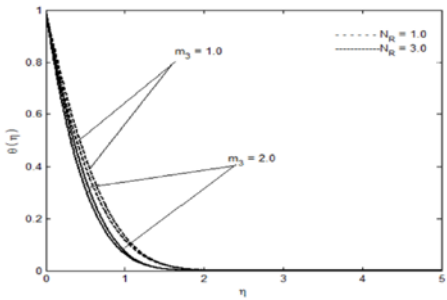

Figure 9
Temperature profiles for various values of Wall temperature parameter and Radiation parameter.

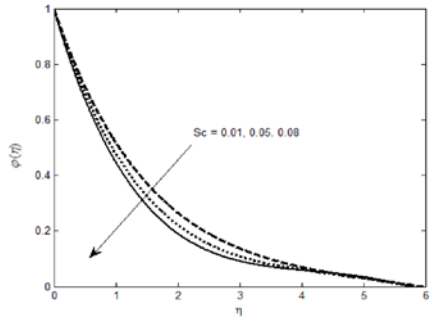

Figure 10
Concentration profiles for various values of Schmidt number.

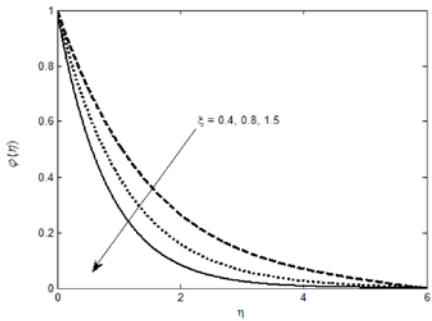

Figure 11
Concentration profiles for various values of chemical reaction parameter.

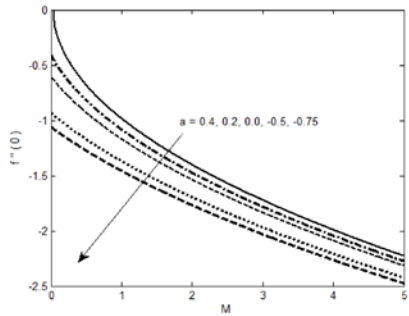

Figure 12
Variation of $f'(0)$ with M for different values of blowing/suction parameter.

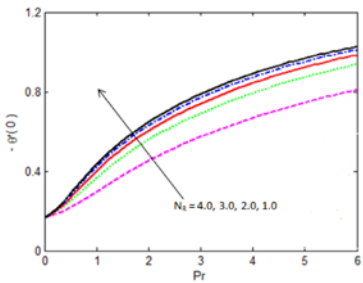

Figure 13
Variation of $-\theta'(0)$ with Pr for different values of radiation parameter.

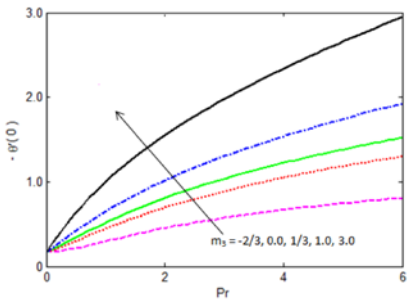

Figure 14
Variation of $-\theta'(0)$ with Pr for different values of wall temperature parameter.

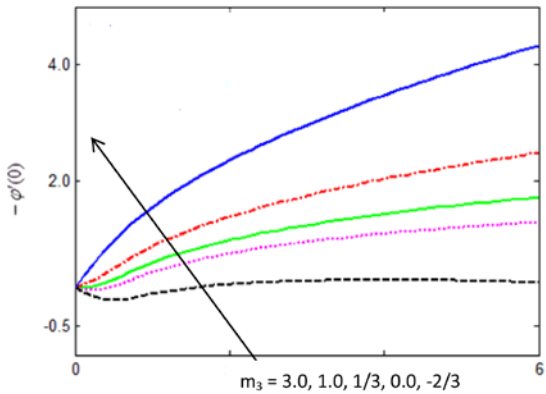

Figure 15
Variation of $-\varphi'(0)$ with *Sc* for different values
of wall temperature parameter.

5. Conclusions

The conclusions of the research paper are as follows:

- Improving values of *M* results in detraction of velocity profiles, whereas reverse trend exhibited for increasing values of *a* and *S*.
- Improving values of *S* and N_R results in detraction of the temperature profile, whereas reverse trend exhibited for increasing values of *M* and *a*.
- Improving values of *S* and *Sc* results in detraction of concentration profile.
- An increase in *a* results in growing values of shearing stress, whereas the reverse happens to rising values of *S* and *M*.
- Increasing values of N_R, *a* and Pr drops the values of the rate of heat transfer.
- Increasing values *a* and *Sh* drops the values of rate of mass transfer while the reverse happens to the increasing value of m_3.

References

1. Sakiadis, B.C.– "Boundary-layer behavior on continuous solid surfaces: I. The boundary-layer equations for two dimensional and axisymmetric flow", AICHE J. **7**, 26-28, (1961).
2. Sakiadis, B.C. – "Boundary-layer behavior on continuous solid surfaces: II. The boundary-layer on a continuous flat surface", AICHE J. **7**, 221-225, (1961).

3. Sakiadis, B.C. – "Boundary-layer behavior on continuous solid surfaces: III. The boundary-layer on a continuous cylindrical surface", AICHE J. **7**, 467-472, (1961).
4. Grubka, L.G. and Bobba, K.M. – "Heat transfer characteristics of a continuous stretching surface with variable temperature", Trans. ASME J. Heat Transfer, **107**, 248-250, (1985).
5. Kumaran, V. and Ramanaih, G. – "A note on the flow over stretching sheet", Arch Mech., **116**, 229-233 (1996).
6. Vajravelu, K.– "viscous flow over a nonlinearly stretching sheet", Appl. Math. Comput., **124(3)**, 281-288, (2001).
7. Elbashbeshy, EMA – "Heat transfer over an exponentially stretching continuous surface with suction", Arch Mech., **53**, 643-651, (2001).
8. Vajravelu, K. and Cannon, J.R. – "Fluid flow over a nonlinearly stretching sheet", Appl. Math. Comput., **181**, 609-618, (2006).
9. Cortell, R. – "Viscous flow and heat transfer over a nonlinearly stretching sheet", Appl. Math. Comput., **184**, 864-873, (2007).
10. Cortell, R. – "Effects of viscous dissipation and radiation on the thermal boundary layer over a nonlinearly stretching sheet", Phys. Lett., **A (372)**, 631-636, (2008).
11. Cortell, R. – "Similarity solutions for the flow and heat transfer of a quiescent fluid over a nonlinearly stretching sheet", J. Mater Process Technol., **203**, 176-183, (2008).
12. Hayat, T., Abbas, Z. and Javed, T. – "Mixed convection flow over nonlinearly stretching sheet", Phys. Lett., **A 372(13)**, 2258-2263, (2008).
13. Hayat, T., Hussain, T. and Javed – "The modified decomposition method and pade approximations for the MHD flow over a nonlinear stretching sheet", Nonlinear Anal–Real world Appl.,**10(2),** 956-973, (2009).
14. Cortell, R. – "Heat and fluid flow due to non-linearly stretching surfaces", Appl. Math. Comput., **217**, 7564-7572, (2011).
15. Shahzad, A., Ali. R. and Khan, M. – "On the exact solution for axisymmetric flow and heat transfer over a nonlinear radially stretching sheet", Chin. Phys. Lett., **29(8)**, 084705, (2012).
16. Mukhopadhyay, S. – "Analysis of boundary layer flow over a porous nonlinearly stretching sheet with partial slip at the boundary", Alexandria Eng. J., **52(4)**, 563-569, (2013).
17. Ferdows, M., Uddin, Md. J. and Afify, A.A.– "Scaling group transformation for MHD boundary layer free convective heat and mass transfer flow past a convectively heated nonlinear radiating stretching sheet," International Journal of Heat and Mass Transfer, **56,** 181-187 (2013).

18. Rashidi, M.M., Rostami, B., Freidoonimehr, N. and Abbasbandy, S. –"Free convective heat and mass transfer for MHD fluid flow over a permeable vertical stretching sheet in the presence of the radiation and buoyancy effects", Ain Shams Engineering Journal, **5**, 901-912, (2014).
19. Cortell, R. – "MHD flow and radiative nonlinear heat transfer of a viscoelastic fluid over a stretching sheet with heat generation/absorption", Energy, **74,** 896-905 (2015).
20. Varshney, C. L. – "Fluctuating flow of Viscous fluid through a porous medium bounded by a porous plate", Indian J. pure Appl. Math.,**10 (12),** 1558-1564, (1979).
21. Vajravelu, K. and Rollins, D. – "Heat transfer in an electrically conducting fluid over a stretching surface", Int. J. Nonlinear Mech., **27 (2),** 265-277, (1992).
22. Afify, A.A. – "MHD free convective flow and mass transfer over a stretching sheet with chemical reaction", Heat Mass Transfer, **40**, 495-500, (2004).
23. Fang, T., Zhang, J. and Yao, S. – "Slip MHD viscous flow over a stretching sheet – an exact solution", Commun. Nonlinear Sci. Numer. Simul., **14**, 3731-3737 (2009).
24. Javed, T., Abbas, Z., Sajid, M. and Ali, N. – "Heat transfer analysis for a hydromagnetic viscous fluid over a non-linear shrinking sheet", Int. J. Heat Mass Transfer, **54**, 2034-2042, (2011).
25. Noor, N.F.M., Abbasbandy, S. and Hashim, I. – "Heat and masstransfer of thermophoretic MHD flowover an inclined radiate isothermal permeable surface in the presence of heat source/sink", Int. J. Heat Mass Transfer, **55**, 2122-2128, (2012).
26. Motsa, S.S. and Sibanda, P. – "On the solution ofMHD flow over a nonlinear stretching sheet by an efficient semi-analytical technique", Int. J. Numer. Meth. Fluids, **68**,1524-1537, (2012).
27. Abbasbandy, S., Roohani, H., Ghehsareh., Hashim, I. – "An Approximate Solution of the MHD Flow over a Non-Linear Stretching Sheet by Rational Chebyshev Collocation Method", U.P.B. Sci. Bull., Series A, **74(4)**, (2012).
28. Kumar, B.R. – "MHD boundary layer flow on heat and mass transfer over a stretching sheet with slip effect", J. Naval Archit. Mar. Eng., **10(2)**, 16-26, (2013).
29. Fadzilah, Md A., Roslinda, N., Norihan, Md, A. and Pop, I. – "Dual solutions in MHD flow on a nonlinear porous shrinking sheet in a viscous fluid", Ali et al. Boundary Value Problems, **32**, (2013).
30. Cortell, R. – "Effects of viscous dissipation and radiation on the thermal boundary layer over a nonlinearly stretching sheet", Phys. Lett., **A 372**, 631-636, (2008).
31. Sajid, M. and Hayat, T. – "Influence of thermal radiation on the boundary layer flow due to an exponentially stretching sheet", Int Comm Heat Mass Transfer, **35**, 347-356, (2008).
32. Chen, T.M. – "Radiation effects on magnetohydrodynamic free convection flow", AIAA J. Thermophys. Heat Transfer, **22(1)**, 125-128, (2008).

33. Pal, D. –"Heat and mass transfer in stagnation-point flow towards a stretching surface in the presence of buoyancy force and thermal radiation", Meccanica, **44**, 145-58, (2009).

34. Ishak, A., Noor, A.,Yacob, A. and Bachok, N.– "Radiation effects on the thermal boundary layer flow over a moving plate with convective boundary condition", Meccanica, **46**, 795-801, (2011).

35. Prasad, V.R., Vasu, B., Beg, O.A. and Parshad, R.D. – "Thermal radiation effects on magnetohydrodynamic free convection heat and mass transfer from a sphere in a variable porosity regime", Commun Nonlinear Sci. Numer Simul., **17**, 654-71, (2012).

36. Chamkha, A.J. – "MHD flow of a uniformly stretched vertical permeable surface in the presence of heat generation/absorption and a chemical reaction", Int. Commun. Heat Mass Transfer, **30**, 413-422, (2003).

37. Afify, A. – "MHD free convective flow and mass transfer over a stretching sheet with chemical reaction", Heat Mass Transfer, **40**, 495-500, (2004).

38. Kandasamy, R., Muhaimin, I. and Khamis, A.B. – "Thermophoresis and variable viscosity effects on MHD mixed convective heat and mass transfer past a porous wedge in the presence of chemical reaction", Heat Mass Transfer, **45,** 703-712, (2009).

39. Bhattacharyya, K. and Layek, G.C. – "Chemically reactive solute distribution in MHD boundary layer flow over a permeable stretching sheet with suction or blowing", Chem. Eng. Commun., **197**, 1527-1540, (2010).

40. Rashad, I.A.M. and El-Kabeir, S.M.M. – "Heat and mass transfer in transient flow by mixed convection boundary layer over a stretching sheet embedded in a porous medium with chemically reactive species", J. Porous Media, **13**, 75-85, (2010).

41. Afify, A.A. and Elgazery, N.S. – "Lie group analysis for the effects of chemical reaction on MHD stagnation-point flow of heat and mass transfer towards a heated porous stretching sheet with suction or injection", Nonlinear Anal. Model. Control., **17**, 1-15, (2012).

INFORMATION TO AUTHORS

Manuscripts should be represent results of original works on theoretical physics on experimental physics with theoretical background or on applied mathematics. Letters to the Editor and Review articles in emerging areas are also published. Submission of the manuscript will be deemed to imply that it has not been published previously and is not under consideration for publication elsewhere (either partly or wholly) and further that, if accepted, it will not be published elsewhere. It is the right of the Editorial Board to accept or to reject the paper after taking into consideration the opinions of the referees.

Manuscripts may be submitted in pdf/MS word format to **admin@itphy.org or susilvcsarkar@yahoo.co.in** Online submission of the paper through our **website: www.itphy.org** is also accepted. The file should be prepared with 2.5 cm margin on all sides and a line spacing of 1.5.

The title of the paper should be short and self-explanatory. All the papers must have an abstract of not more than 200 words, the abstract page must not be a part of the main file. Abstract should be self-contained. It should be clear, concise and informative giving the scope of the research and significant results reported in the paper. Below the abstract four to six key words must be provided for indexing and information retrieval.

The main file should be divided into sections (and sub-sections, if necessary) starting preferably with introduction and ending with conclusion. Displayed formula must be clearly typed (with symbols defined) each on a separate line and well-separated from the adjacent text. Equations should be numbered with on the right-hand side consecutively throughout the text. Figures and Tables with captions should be numbered in Arabic numerals in the order of occurrence in the text and these should be embedded at appropriate places in the text. Associated symbols must invariably follow SI practice.

References should be cited in the text by the Arabic numerals as superscript. All the references to the published papers should be numbered serially by Arabic numerals and given at the end of the paper. Each reference should include the author's name, title, abbreviated name of the journal, volume number, year of publication, page numbers, as in the simple citation given below :

For Periodicals : Sen, N.R. – On decay of energy spectrum of Isotopic Turbulence, J. Appl. Phys. **28,** No.10, 109-110 (1999).

1. Mikhilin, S. G. – Integral Equations , Pergamon Press, New York (1964).
2. Hinze, A. K. – Turbulence Study of Distributed Turbulent Boundary Layer Flow, Ph.D, Thesis, Rorke University (1970).

The corresponding author will receive page proof, typically as a pdf file. The proof should be checked carefully and returned to the editorial office within two or three days.Corrections to the proof should be restricted to printing errors and made according to standard practice. At this stage any modifications (if any) made in the text should be highlighted.

To support the cost of publication of the journal, the authors (or their Institutions) are requested to pay publication charge Rs.200/- per printed page for authors of Indian Institutes and US$ 20 for others. Publication charges to be sent directly to **CALCUTTA INSTITUTE OF THEORETICAL PHYSICS, 'BIGNAN KUTIR', 4/1, MOHAN BAGAN LANE, KOLKATA-700 004, INDIA**.

A pdf of the final publisher's version of the paper will be sent to the corresponding author shortly after print publication by our co-publisher, **Wilcox Books & Periodicals Co. (wilcoxbooks@gmail.com)**

All communications are to be sent to the Secretary, Calcutta Institute of Theoretical Physics, 'Bignan Kutir', 4/1, Mohan Bagan Lane, Kolkata-700 004.

Indian Journal of Theoretical Physics is in the list of Journals approved by UGC.

For details please visit our website www.itphy.org

PUBLICATIONS
OF
CALCUTTA INSTITUTE OF THEORETICAL PHYSICS

"BIGNAN KUTIR"

4/1, Mohan Bagan Lane, Kolkata – 700 004, India

Phone : +91-33-25555726

INDIAN JOURNAL OF THEORETICAL PHYSICS (ISSN : 0019-5693)

Research Journal containing Original Papers, Review Articles and Letters to the Editor is published quarterly in March, June, September and December and circulated all over the world.

Subscription Rates

₹ 1500 per volume (for Bonafide Indian Party)
US $ 350 (for Foreign Party)

Back Volume Rates

₹ 1500 per volume (for Bonafide Indian Party)
US $ 350 per volume or Equivalent Pounds per volume

Books Written by Prof. K. C. Kar, D. Sc.

- **INTRODUCTION TO THEORETICAL PHYSICS**
  [Vol. 1 and Vol. II (Accoustics)]
  Useful to students of higher physics
  Price : ₹ 60 or US $ 10 per volume
- **WAVE STATISTICS : Its principles and Applications**
  [Vol. I and Vol. II]
  Useful to Post Graduate and Research students
  Price : ₹ 80 or US $ 12
- **STATISTICAL MECHANICS : Principles and applications**
  [Vol. I and Vol. II]
  Useful to Advanced students of Theoretical Physics
  Price : ₹ 120 or US $ 15
- **A NEW APPROACH TO THE THEORY OF RELATIVITY**
  Useful to post Graduate and Advanced students
  Price : ₹ 50 or US $ 8

Order may be sent directly to Calcutta Institute of Theoretical Physics
"Bignan Kutir", 4/1, Mohan Bagan Lane, Kolkata – 700 004, India

---

Unimage, 10, Roy Bagan Street, Kolkata- 700 006 and published by Dr. S. K. Sarkar, Secretary, on behalf of Calcutta Institute of Theoretical Physics, 4/1, Mohan Bagan Lane, Kolkatta – 700 004, India.

Detailed information about our other Journals

1. Name of the Journal : **Bengal Past & Present**
   ISSN :..... **0005-8807**
   Frequency:..... **Annually (Latest Vol. 136,2017)**
   Price: .....(a) In India: Institutions: **500-00**
   .....(b) Overseas : **$ 150-00**
   Postage:..... **Post Free**
   * Discount :.... To Subscription Agencies: **25%**
   ..... To Institutions :..... **Fixed Price**
2. Name of the Journal:..... **Journal of the Indian Anthropological Society**
   ISSN :..... **0019-4387**
   Frequency:..... **Three Issues in a year (March, July & November)**
   Price:..... (a) In India: Institutions: **1500-00 (Latest Vol. 51, 2016)**
   ..... (b) Overseas..... **$ 300-00**
   Postage:..... **Post Free**
   * Discount: To Subscription Agencies: **25%**
   ..... To Institutions :..... **Fixed Price**
3. Name of the Journal: ..... **Journal of Surface Science and Technology**
   ISSN :..... **0970-1893**
   Frequency:..... **Quarterly**
   Price:..... (a) In India: Institutions: **1800-00 (Latest Vol. 33, 2017)**
   ..... (b) Overseas..... **$ 300-00**
   Postage :.....**Post Free**
   * Discount: To Subscription Agencies: **25%**
   ..... To Institutions :..... **Fixed Price**
4. Name of the Journal: **The Journal of the Indian Academy of Philosophy**
   ISSN: .....
   Frequency:..... **Bi-Annual**
   Price:..... (a) In India: Institutions: **200-00 (Latest Vol. 52, 2013)**
   ..... (b) Overseas..... **$ 30-00**
   Postage :..... **Post Free**
   * Discount :... To Subscription Agencies: **25%**
   ..... To Institutions :..... Fixed Price
5. Name of the Journal: **The Quarterly Review of Historical Studies**
   ISSN:..... 0033-5800
   Frequency:..... **Quarterly**
   Price:..... (a) In India: Institutions: **1500-00 (Latest Vol. 57, 2017-18)**
   ..... (b) Overseas..... **$ 400-00**
   Postage:..... **Post Free**
   * Discount :... To Subscription Agencies: **25%**
   ..... To Institutions: **Fixed Price**
6. Name of the Journal: **Indo-Iranica**
   ISSN:.....03789-0856
   Frequency:..... **Quarterly**
   Price:..... (a) In India: Institutions: **1500-00 (Latest Vol. 69, 2016)**
   ..... (b) Overseas..... **$ 350-00**
   Postage:.....**Post Free**
   * Discount : To Subscription Agencies: **25%**
   ..... To Institutions :..... **Fixed Price**

For more Journals Visit our website : www.wilcoxjournals.com

*** For Foreign Subscriptions Only**

Order should be sent to :

Wilcox Books and Periodicals Co.
8/2/A, Neogi Para Road,
Kolkata - 700036 (India)
Email : wilcoxbooks@gmail.com
: wilcoxbooks@yahoo.co.in